POLITECNICO
MILANO 1863

SCUOLA DI INGEGNERIA INDUSTRIALE
E DELL'INFORMAZIONE

Kinetic modeling of deactivation over methanation catalysts

Tesi di Laurea Magistrale in
Chemical Engineering - Ingegneria Chimica

Alraghib Eisa Ishag Shogar, 10947936

Abstract: Catalyst deactivation by **Boudouard coking** limits the operational lifetime of fixed-bed CO methanation reactors for synthetic natural gas production from biomass-derived syngas. The strongly exothermic nature of methanation leads to localized temperature peaks, or **hotspots**, which accelerate carbon deposition. The pseudodynamic modelling framework recently introduced by *Pappagallo et al. (2025)* can predict the time-dependent conversion loss due to coking by decoupling slow deactivation kinetics from fast transport phenomena, but the original study was restricted to a narrow range of inlet temperatures and a single reactor configuration. This thesis extends the pseudodynamic model to a comprehensive **seven-parameter sensitivity analysis** on a plate-cooled fixed-bed geometry, covering inlet temperature (300–360°C), coolant temperature (280–340°C), heat transfer coefficient ($U \times 0.35$–0.80 relative to the baseline of 50 W m^{-2} K^{-1}), total pressure (8–20 bar), gas hourly space velocity ($GHSV$, 500–2000 h^{-1}), H_2/CO feed ratio (2.0–3.5), and inlet steam fraction (0–7 mol%). Deactivation is quantified via the time required for outlet CO conversion to fall below 25% (t_{25}). Additionally, three catalyst packing configurations—cylindrical pellets, monolithic honeycomb, and open-cell foam—are compared through their characteristic overall heat transfer coefficients. The **heat transfer coefficient** and **inlet temperature** are identified as the most influential parameters. Reducing U to 0.35× baseline shortens t_{25} from 131.3 to 18.2 h (7.2×reduction), while raising T_{in} from 300 to 360°C reduces it by 58%. Total pressure (8 → 20 bar, −62%) and $GHSV$ (500 → 2000 h^{-1}, −90%) strongly accelerate deactivation. Conversely, steam co-feeding (+31% at 7 mol%) and excess hydrogen (+29% at H_2/CO = 3.5) extend lifetime at modest operational cost. The **open-cell foam** ($U = 250$ W m^{-2} K^{-1}) achieves $t_{25} = 459.6$ h—a 3.64-fold improvement over the packed-bed baseline (126.3 h)—driven by a 73°C hotspot reduction and suppression of hotspot migration. The **monolithic honeycomb** reaches 343.4 h (2.72× improvement). These results demonstrate that **structured catalyst supports**, combined with optimized feed composition, constitute the most effective strategy for extending catalyst lifetime in fixed-bed CO methanation. The findings confirm the pseudodynamic framework as a practical and computationally efficient tool for reactor-scale deactivation analysis and thermal management optimization.

Advisor:
Prof. Emanuele Moioli

Academic year:
2025-2026

Key-words: CO methanation • catalyst deactivation • Boudouard coking • pseudodynamic model • fixed-bed reactor • hotspot suppression • structured catalyst supports • open-cell foam • monolithic honeycomb • parametric sensitivity analysis

1. Introduction

1.1. Background and Industrial Context

The world needs to work together to cut down on greenhouse gas emissions and switch to energy sources that do not create carbon. Chemical engineering needs to find strategies to turn gases into chemicals. Catalytic methanation changes carbon oxides (CO and CO_2) into synthetic natural gas (SNG). The current strategic objective of this project is to integrate renewable electricity into the existing energy infrastructure [3, 29]. The Power-to-Gas (PtG) idea uses the methanation reaction to chemically store renewable energy. This method makes hydrogen by breaking water down into hydrogen and oxygen. It uses extra electricity from solar or wind energy systems. Then, carbon oxides are added to hydrogen to make methane. You can put this methane right into pipelines and storage facilities that already have natural gas in them [20]. Methanation can do more than merely turn energy into gas. Biomass gasification makes syngas, which is largely carbon monoxide (CO), hydrogen (H_2), carbon dioxide (CO_2), and other things that are not healthy for the environment. Using catalytic methanation, syngas is turned into synthetic natural gas (SNG), which creates a fuel cycle that doesn't add any carbon to the air [18, 33]. There are no CO_2 emissions when you consume synthetic natural gas (SNG) made from biomass. Carbon is released when anything burns. During photosynthesis, plants absorb this same carbon [3, 20]. Direct air capture (DAC) technologies provide an alternate means for obtaining CO_2, hence facilitating methanation as a carbon usage approach within a unified circular carbon economy [19]. Figure 1 shows how power and gas work together to make methanation possible, which is what makes a carbon-neutral cycle conceivable.

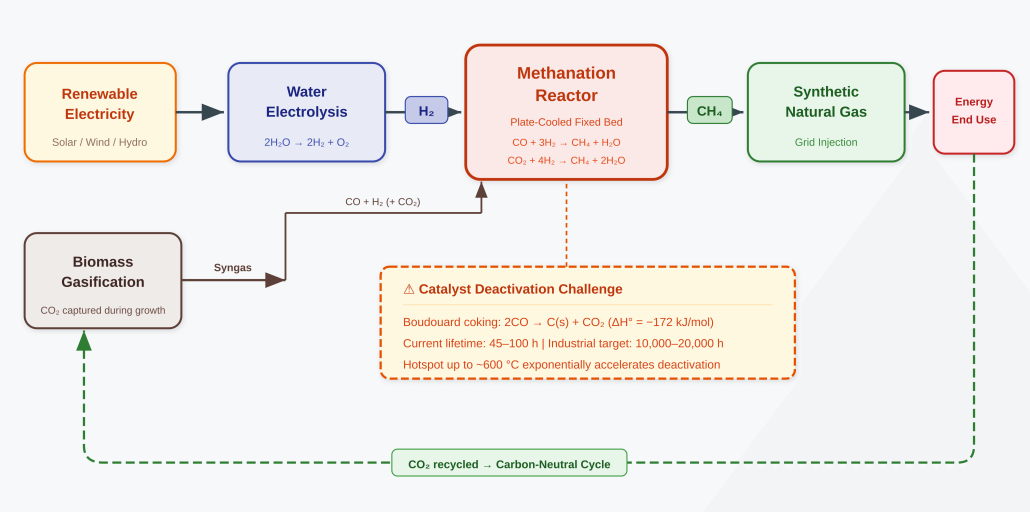

Figure 1: Power-to-Gas strategy for carbon-neutral synthetic natural gas generation, featuring the catalyst deactivation issue with Boudouard coking.

The CO methanation (1) and CO_2 methanation (2) reactions, commonly known as the Sabatier reaction, constitute the primary stages of methane production. Both reactions release significant heat and operate effectively at high pressure and moderate temperature.

$$CO + 3H_2 \rightleftharpoons CH_4 + H_2O \qquad \Delta H^\circ_{298} = -206.1 \text{ kJ/mol} \tag{1}$$

$$CO_2 + 4H_2 \rightleftharpoons CH_4 + 2H_2O \qquad \Delta H^\circ_{298} = -164.9 \text{ kJ/mol} \tag{2}$$

The water-gas shift (WGS) reaction (Equation 3) occurs concurrently with other reactions and significantly influences the overall conversion and product distribution in mixed-feed systems:

$$CO + H_2O \rightleftharpoons CO_2 + H_2 \qquad \Delta H^\circ_{298} = -41.2 \text{ kJ/mol} \tag{3}$$

Nickel-based catalysts supported on alumina (Ni/Al_2O_3), zirconia (Ni/ZrO_2), or mixed oxides are optimal for industrial methanation due to their high activity, favorable selectivity for methane, and relative cost-effectiveness compared to noble metals such as ruthenium and rhodium [2, 16]. However, constructing and operating reactors is difficult due to the significant heat generated during methanation. Enterprises typically employ fixed-bed

reactors. The reaction generates substantial heat, resulting in elevated temperatures in certain regions of the reactor. This is particularly applicable in the kinetic zone, where the reactants are most densely concentrated [14].

Moioli et al. [21] assert that plate-cooled fixed-bed reactors are an excellent method for managing this heat release. The rationale for this is that they cease functioning when the thermal flow is interrupted. The methanation reaction is well understood from a technical perspective. However, a significant issue persists with the application of fixed-bed methanation reactors in industry for converting syngas into methane: the catalysts deactivate too rapidly. This phenomenon represents the principal challenge addressed in this thesis.

1.2. The Catalyst Deactivation Challenge

Catalyst deactivation is the gradual decline in catalytic activity and selectivity over time during operation. A multitude of physical and chemical factors may contribute to this phenomenon. Thermal sintering, poisoning by feed contaminants (particularly sulfur compounds), and carbon deposition or coking [8, 27] are the primary factors that can inactivate the active metal phase during methanation. The cleaning of gas upstream can contribute to minimizing the risk of poisoning [21, 31], and sintering is typically a concern at elevated temperatures. Carbon deposition remains the predominant and most effective method of regulating CO methanation in standard industrial settings [28].
The discrepancy between the necessary and actual catalyst lives demonstrates the severity of this problem. The cost-effectiveness of industrial methanation systems is contingent upon the durability of their catalysts, which must endure between 10,000 and 20,000 hours of operation. However, recent modeling by Pappagallo et al. [28] on fixed-bed CO methanation reactors demonstrated that it requires only 45 to 100 hours to reach critical deactivation, defined as the point at which CO conversion falls below 25%. These conditions are defined as normal operating conditions, which include inlet temperatures ranging from 300 to 360°C, an inlet pressure of 8 bar, and a stoichiometric 3:1 H_2/CO feed. This discrepancy is of the order of magnitude of two to three, underscoring the critical importance of comprehending, anticipating, and regulating the deterioration of catalysts within methanation reactors.

The economic ramifications of such a precipitous cessation are deleterious. The replacement of catalysts can result in increased operational costs, lead to periods of downtime, and generate waste. The process is challenging to regulate and plan for long-term production due to the difficulty in predicting the rate of deactivation. To address this challenge, it is imperative to develop enhanced methodologies for the synthesis of catalysts and to cultivate a comprehensive understanding of how the parameters and configurations of reactors influence the spatiotemporal progression of deactivation. The acquisition of this information is only possible through models that have undergone testing.

1.3. State of the Art

1.3.1 Carbon Deposition Mechanisms in CO Methanation

Carbon buildup on methanation catalysts is a complicated process that happens when many separate reactions happen at the same time. The Boudouard reaction, sometimes called CO disproportionation, happens most when there is a lot of CO. Equation 4 shows it:

$$2\mathrm{CO} \rightleftharpoons \mathrm{C_{(s)}} + \mathrm{CO_2} \qquad \Delta H^\circ_{298} = -172 \text{ kJ/mol} \tag{4}$$

This reaction is thermodynamically better at temperatures below about 700°C [1]. It also creates solid carbon (coke) that builds up on the active catalytic surface, blocking active sites and slowing down the reaction rate. There are more ways to generate carbon, like (Equation 5), which illustrates how hydrogen can break down CO, and (Equation 6), which demonstrates how methane can break down:

$$\mathrm{CO} + \mathrm{H_2} \rightleftharpoons \mathrm{C_{(s)}} + \mathrm{H_2O} \qquad \Delta H^\circ_{298} = -131.3 \text{ kJ/mol} \tag{5}$$

$$\mathrm{CH_4} \rightleftharpoons \mathrm{C_{(s)}} + 2\mathrm{H_2} \qquad \Delta H^\circ_{298} = +74.8 \text{ kJ/mol} \tag{6}$$

The morphology and structure of the deposited carbon exhibit considerable variation based on the local reaction conditions, the characteristics of the catalyst, and the composition of the gas phase. Mutz et al. [24] employed operando Raman spectroscopy to demonstrate that carbonaceous deposits on catalytic surfaces exhibit diverse structural orders, from amorphous carbon to partially graphitized species, with the degree of ordering significantly influenced by the formation temperature and catalyst composition. When the temperature is below

400°C, most of the carbon and polymeric carbon species that develop are amorphous. Graphitic structures that are more structured form at higher temperatures. Gasification is not a good way to get rid of these structures [27]. Figure 2 shows all the ways that carbon can build up on catalysts that make methane from nickel. It shows the reaction routes and the important things that make the process go faster.

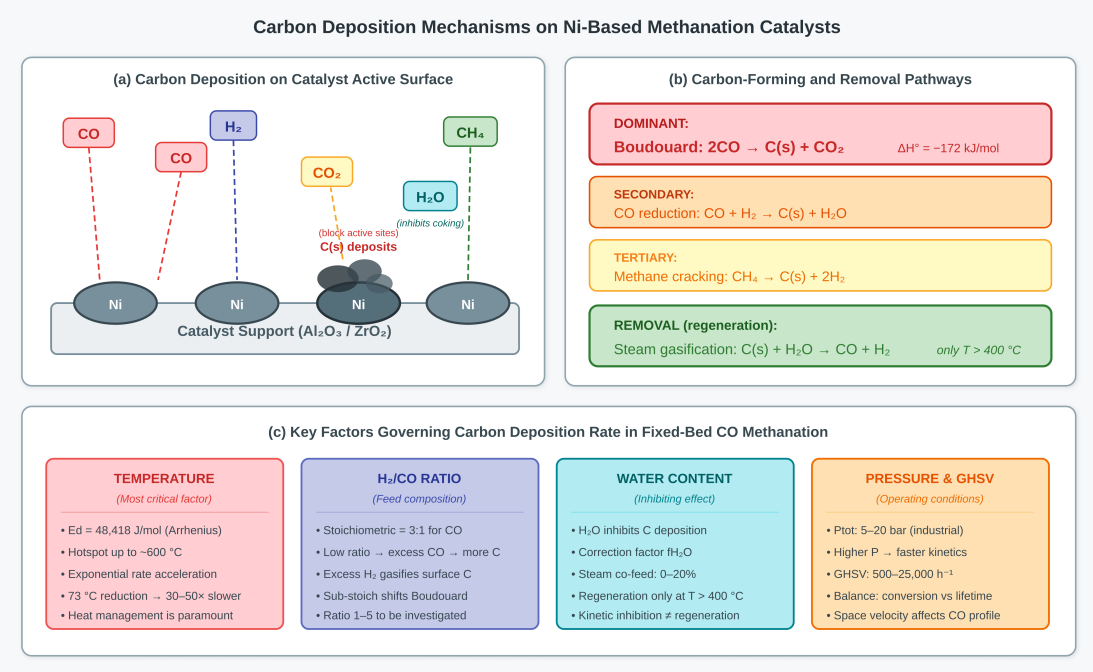

Figure 2: Carbon deposition mechanisms on Ni-based methanation catalysts: (a) coke formation on the active surface, (b) carbon-forming and removal reaction pathways, (c) key governing factors

A comprehensive evaluation of the rate and extent of carbon accumulation in CO methanation systems necessitates consideration of numerous salient factors. Temperature is the most significant factor in this regard. The Boudouard reaction rate increases exponentially with temperature, according to Arrhenius kinetics, with an apparent activation energy of approximately 48 kJ/mol [28, 34]. This temperature sensitivity exerts a substantial influence on the functionality of fixed-bed reactors. For instance, localized hotspots can reach temperatures as high as 600°C, which have been shown to expedite carbon deposition in the reactor's input kinetic zone [28].

The H_2/CO ratio in the feed gas is also of significant importance. Sub-stoichiometric ratios ($H_2/CO < 3$ for CO methanation) have been shown to raise the local CO partial pressure and move the Boudouard equilibrium toward carbon production. On the other hand, too much hydrogen speeds up the gasification of carbon that has already been deposited and slows down the net accumulation of carbon [2, 32]. The partial pressure of water vapor significantly hinders carbon deposition, as water may convert surface carbon species into gas at high temperatures via the reaction:

$$C + H_2O \rightarrow CO + H_2 \tag{7}$$

This inhibitory mechanism has been empirically quantified using correction factors that decrease the deactivation rate when the local water content rises [28, 32]. It is essential to distinguish between the kinetic inhibition of carbon deposition by water during standard operation (which occurs at all temperatures) and the actual regeneration of a coked catalyst through steam gasification, which requires temperatures exceeding 400°C [31, 34].

From an industrial perspective, the reversibility of coking-induced deactivation via steam regeneration is a crucial characteristic. Zhang et al. [34] demonstrated that spent catalyst from methanation reactors may be repurposed through coke gasification using steam. Schildhauer and Biollaz [31] claimed that adding steam to industrial methanation plants regularly is a common technique to recycle the catalyst. But using regeneration cycles makes things more complicated and can cause performance problems from time to time. This makes it a far better idea to stop or lower carbon buildup by improving the way things work.

1.3.2 Deactivation Kinetics: Models and Approaches

To quantitatively characterize catalyst deactivation, we require kinetic models that can mathematically correlate the rate of activity loss with the existing catalytic activity, temperature, gas composition, and specific operating conditions. The literature has yielded two primary categories of deactivation kinetic models: mechanistic models founded on fundamental surface reaction stages and empirical or semi-empirical power-law models.

Mechanistic Models

Mechanistic deactivation models rely on the establishment of quasi-stationary kinetic processes for the distinct phases involved in the coke formation process at catalytic active sites. Ostrovskii [26, 27] developed an extensive framework for linear mechanisms of catalyst deactivation. This method uses the local gas-phase composition to figure out the coverage fractions of intermediate surface species. The total deactivation rate is the consequence of the competition between processes that add carbon and those that take it away from the surface. Mechanistic models are accurate and help us understand how deactivation works, but they usually contain a lot of factors and difficult math that make it considerably more expensive to run simulations on a reactor scale [28].

Power-Law and Semi-Empirical Models

Ostrovskii [27] and Sun et al. [32] investigated models for power-law deactivation. These models illustrate the variation in the deactivation rate influenced by power-law factors associated with the operational variables and the prevailing activity:

$$\frac{d\alpha}{dt} = -k_d \cdot P_{CO}^{\alpha} \cdot f_{H_2O} \cdot \alpha^{\beta} \tag{8}$$

Where α is the catalyst activity (the ratio of the current reaction rate to the fresh-catalyst reaction rate at the same conditions), k_d is the temperature-dependent deactivation rate constant following an Arrhenius relationship, P_{CO} is the partial pressure of CO, α is the apparent reaction order with respect to CO, f_{H_2O} is a correction factor that takes into account the inhibiting effect of water on carbon deposition, and β is the activity influence parameter.
Sun et al. [32] changed this model for use in Sabatier reactors by adding a water correction factor that considers how steam affects carbon deposition. Pappagallo et al. [28] subsequently modified the parameters of this model for CO methanation, enhancing its efficacy. They calculated the kinetic parameters using experimental data from Zhang et al. [34] obtained from a laboratory-scale reactor operating at temperatures ranging from 320 to 360°C. The modified Arrhenius expression (Equation 9) illustrates the variation of the deactivation rate constant with temperature:

$$k_d = k_{d,0} \cdot \exp\left(-\frac{E_d}{R \cdot T}\right) \tag{9}$$

Ostrovskii [27] demonstrated that the power-law technique is effective for most experimental deactivation datasets, circumventing the complex mathematics associated with mechanistic theories. This is the best way to research how to improve reactors on a large scale. Celoria et al. [2] just put out a full kinetic study of the methanation of CO and CO_2 mixed syngas on Ni/Al_2O_3. The study looked at deactivation phenomena and found that Boudouard-based coking is the best way to deactivate in places with a lot of CO. Chapter 2 will go into more detail about the complete mathematical formulation and the specific calibrated parameters used in this study.

1.3.3 Validated Reaction Kinetics for CO and CO_2 Methanation

For any reactor-scale model, it is essential to possess validated intrinsic kinetic models for the three concurrent processes in CO methanation systems: CO methanation, CO_2 methanation, and the water–gas shift reaction. The kinetic equations in the reference framework for this thesis are based on two independently validated experiments. Koschany et al. [15] developed a Langmuir–Hinshelwood–Hougen–Watson (LHHW) kinetic model for CO_2 methanation on a coprecipitated $Ni/Al(O)_x$ catalyst. They utilized 555 K as their reference temperature. The model includes the competitive adsorption of hydrogen, water, and CO_2 onto the surface of the catalyst. It also accounts for thermodynamic equilibrium and explains how equilibrium is reached when the temperature and concentration of the products are high.

Kopyscinski et al. [14] utilized a catalytic plate reactor to evaluate concentration and temperature at different coordinates. They used these data to create kinetic equations for the water-gas shift process and CO methanation, with 598.15 K as the temperature of reference. Their research produced the initial kinetics for CO

methanation, later corroborated by spatially resolved data from a fixed-bed reactor. This made it possible to make accurate predictions for temperature profiles and axial conversion [28]. The combination of these kinetic models forms the reaction kinetic submodel used in the present thesis, covering the three simultaneous reactions listed in Table 1.

j	Reaction	Chemical Equation	ΔH°_{298} (kJ/mol)
1	CO_2 methanation	$CO_2 + 4H_2 \rightleftharpoons CH_4 + 2H_2O$	-164.9
2	Water–gas shift	$CO + H_2O \rightleftharpoons CO_2 + H_2$	-41.2
3	CO methanation	$CO + 3H_2 \rightleftharpoons CH_4 + H_2O$	-206.1

Table 1: Reactions in the kinetic submodel [14, 15].

1.3.4 Pseudodynamic Modelling of Catalyst Deactivation in Fixed-Bed Reactors

The pseudodynamic framework created by Pappagallo et al. [28] is a key methodological contribution to the modeling of catalyst deactivation in fixed-bed reactors. This approach exploits the fundamental separation of time scales between the fast reactor phenomena (reaction kinetics and heat/mass transport, occurring on a time scale of seconds) and the slow catalyst deactivation (occurring over hours to hundreds of hours). By recognizing that the reactor achieves a quasi-steady state at any given instant in the deactivation process, the pseudodynamic model avoids the need to solve coupled partial differential equations in both space and time. Instead, the model consists of a single ordinary differential equation (ODE) in time for the catalyst activity, coupled with a steady-state reactor submodel that is called at each integration step to compute the axial profiles.

The deactivation rate is computed from the current profiles, the activity is updated, and a new steady-state solution is obtained at the slightly lower activity. The detailed mathematical formulation and MATLAB® implementation of this framework will be presented in Chapter 2. The pseudodynamic model showed several important physical effects in CO methanation with a fixed bed. The most important thing is that the deactivation happens in a wave-like way through the reactor. The catalyst at the inlet kinetic zone, which is the part of the system that gets the hottest and has the most CO, stops working first. The reaction front and its hotspot move downstream when this zone is no longer active. This turns off the next part of the catalyst bed. This makes a moving deactivation front that moves through the reactor over time. The outlet conversion stays the same until the deactivation front gets to the thermodynamic zone, then it starts to go down [28].

The deactivation wave and moving hotspot phenomena are shown in 5 and 6. These figures are recommended for reproduction in this chapter. Froment [8] previously elucidated deactivation phenomena at both the particle and reactor scales, while Froment and Bischoff [9] furnished critical kinetic data for fixed-bed reactors undergoing catalyst fouling. Cordero-Lanzac et al. [4, 5] developed a model to quantify the rapid deterioration of catalysts in isothermal reactor setups.

The pseudodynamic framework developed by Pappagallo et al. [28] is distinctive in its ability to manage slow deactivation over extended periods (hundreds of hours) with minimal computational demand. It is sufficient to employ a single ordinary differential equation (ODE) for each reaction. This renders it an optimal selection for the comprehensive parametric optimization studies conducted in this thesis.

1.3.5 Operando Characterization of Coking in Methanation Catalysts

The experimental characterization of carbon deposition on methanation catalysts has been markedly enhanced through the utilization of operando and in situ spectroscopic techniques, notably Raman spectroscopy. Operando Raman spectroscopy facilitates real-time observation of carbon species formation on catalytic surfaces under genuine reaction conditions, offering mechanistic insights into the characteristics and dynamics of coke deposition [24].

Mutz et al. [24] used operando Raman spectroscopy to study CO_2 methanation with Ni/Al_2O_3, Ni_3Fe, and $NiRh_{0.1}$ catalysts. They found that carbon production could be a way to deactivate the catalysts and linked the properties of the carbon species produced to the catalyst composition and reaction conditions. Mutz et al. [22, 23] conducted complementary operando X-ray absorption spectroscopy studies, thereby providing further evidence that surface oxidation and carbon deposition occur dynamically when reaction conditions change. This suggests that the transient operation of methanation reactors, an unavoidable aspect of PtG applications, may

exacerbate deactivation.

Building on these findings, Celoria et al. [2] conducted a detailed kinetic analysis of the processes that deactivate Ni/Al_2O_3 catalysts when CO_2 and CO mixed syngas are methanated. This finding provides further evidence that carbon deposition and reaction kinetics are indeed interconnected phenomena. Engeldinger et al. [7] and Nuguid et al. [25] have advanced operando Raman methods for studying how catalysts change structure and redox dynamics while they are reacting.

The analysis of coke deposits utilized on catalysts by ex-situ methodologies remains a crucial supplemental technique. Pappagallo et al. [28] demonstrated significant variations in the type and quantity of carbon deposition based on its location within the reactor. This backed up the hypothesis of a deactivation wave. The hotspot is the area with the most carbon loading. These computer-based conclusions are consistent with findings in experimental literature regarding coke deposition profiles. They also highlight how crucial it is to use approaches that look at space to figure out how long a catalyst will last and how to plan for that.

1.3.6 Effect of Reactor Configuration on Heat Transfer and Catalyst Lifetime

The arrangement of the reactor and catalyst packing is particularly crucial for how long the catalyst lasts because temperature has such a huge effect on how rapidly carbon builds up. The total heat transfer coefficient "U" has a direct effect on the magnitude of the temperature hotspot, which in turn impacts the local deactivation rate. This discovery leads to the search for new ways to pack catalysts that have better thermal conductivity.

There are three basic types of fixed-bed catalysts that can make methane. They all move heat in different ways:

- **Randomly Packed Beds:** The industrial baseline is made up of a regular packed bed of catalyst pellets deposited in random spots. This kind of bed has heat transmission coefficients ranging from 40 to 80 $W/m^2 \cdot K$ [6]. The plate-cooled fixed-bed reactor model by Pappagallo et al. [28] has a heat transfer coefficient of 50 $W/m^2 \cdot K$, which is the same as this baseline value and serves as the standard model for this thesis. While cost-effective, it lacks efficient radial heat transfer, leading to hotspots.

- **Open-cell Foam Structures:** These consist of metallic (e.g., FeCrAlloy) or ceramic foams covered with a catalytically active washcoat. Giani et al. [10] found that metallic foams might move heat 3 to 10 times better than packed beds, while Incera Garrido et al. [13] noted thermal conductivity improvements of 5 to 15 times. Richardson et al. [30] discovered that these structures might reduce hotspots by 100 to 200°C compared to conventional beds.

- **Monolithic Honeycombs:** These parallel-channel structures exhibit high geometric surface areas (200–900 m^2/m^3) and great axial heat conduction. Hayes et al. [12] stated that monolithic structures exhibited heat transfer coefficients 2 to 4 times superior to packed beds. Groppi and Tronconi [11] demonstrated that hotspot temperatures could be reduced by 50–100°C, suggesting catalysts could last approximately 2.7 times longer [28].

The quantitative correlation between improved heat transfer and prolonged catalyst lifespan is substantial. The Arrhenius-type temperature dependence of the Boudouard deactivation kinetics, with an activation energy of 48,418 J/mol [28], indicates that a reduction in hotspot temperature of 73°C (feasible with foam structures) corresponds to an approximate 30–50-fold decrease in the local deactivation rate at the hotspot location. Nonetheless, a comprehensive comparison of catalyst longevity across these configurations under uniform methanation conditions has yet to be documented in the public domain. Table 2 summarizes the key characteristics and expected performance of the three configurations.

Parameter	Packed Bed	Monolith	Open-Cell Foam
U [$W/m^2 \cdot K$]	50 (1×)	150 (3×)	250 (5×)
T_{max} (fresh) [°C]	∼612	∼570	∼539
Expected lifetime [h]	∼126	∼343 (2.7×)	∼460 (3.6×)

Table 2: Comparison of catalyst packing configurations for CO methanation [6, 10–12, 28, 30].

1.4. Critical Gaps

The preceding state-of-the-art review reveals that while validated kinetic models for both the methanation reactions [14, 15] and the coking deactivation mechanism [32, 34] exist in the literature, and the pseudodynamic modelling framework of Pappagallo et al. [28] has demonstrated its capability to predict catalyst deactivation in fixed-bed reactors, several critical research gaps collectively prevent the rational optimization of catalyst lifetime in industrial CO methanation.

1.4.1 Gap 1: Limited Parametric Exploration for CO Methanation Coking

The pseudodynamic modelling framework of Pappagallo et al. [28] was validated and demonstrated with a limited set of operating conditions: inlet temperatures of 300–360°C (a 60°C range), a single heat transfer coefficient (U = 50 W/m^2·K), a single total pressure of 8 bar, and a fixed gas hourly space velocity (GHSV) of 500 h^{-1}. The narrow temperature range explored is insufficient to identify the optimal inlet temperature that balances high initial conversion against acceptable deactivation rates. Critical unanswered questions regarding the effects of pressure, space velocity, H_2/CO ratio, or steam co-feeding on the spatiotemporal evolution of deactivation in CO methanation fixed-bed reactors include:

- What is the optimal T_{in} and T_e, considering both catalytic activity and deactivation rate?
- Can enhanced heat removal (higher U) suppress hotspot formation and extend catalyst lifetime?
- How does P_{tot} modulate the Boudouard equilibrium and carbon deposition rates?
- What is the optimal GHSV that balances conversion and catalyst lifetime?
- How do the H_2/CO ratio and steam co-feeding affect the deactivation kinetics?

1.4.2 Gap 2: Absence of Reactor Bed Configuration Comparison

While foam and monolithic catalyst structures have been proven to enhance heat transfer, as fully described in the literature on general catalysis [10–12, 30], this investigation quantifies the effect of these improved heat transfer properties on catalyst lifetime, specifically in CO methanation. The correlation between hotspot suppression and the pace of deactivation wave propagation under methanation-specific settings has yet to be investigated. Key questions remain:

- How does better heat transfer in foam and solid structures change the way hotspots form?
- What is the quantitative catalyst lifespan for each configuration under identical operating conditions?

1.5. Research Opportunity and Two-Stage Approach

This thesis addresses the acknowledged shortcomings by conducting a comprehensive parametric study and catalyst packing configuration analysis of catalyst deactivation in fixed-bed CO methanation reactors, employing the validated pseudodynamic modelling framework [28] with explicit Boudouard-based coking kinetics.

1.5.1 Comprehensive Parametric Analysis

This study systematically varies key operating parameters within industrially relevant ranges, extending significantly beyond those examined in the literature. The following research questions and parameter ranges are defined to guide this investigation as shown in Table 5: inlet temperature T_{in} (250–450°C), heat transfer coefficient U (10–1000 W/m^2·K, encompassing passive cooling to active heat exchange), coolant temperature T_e (200–400°C), total pressure P_{tot} (5–20 bar), gas hourly space velocity $GHSV$ (500–25,000 h^{-1}), H_2/CO molar ratio (1–5, from sub-stoichiometric to excess hydrogen), and steam mole fraction (0–20% for coking suppression).

1.5.2 Catalyst Packing Configuration Comparison

We looked into three different catalyst packing configurations using heat transfer coefficients from the literature applied to the same reactor shape: conventional packed bed (U = 50 W/m^2·K [6, 28]), open-cell foam (U = 250 W/m^2·K [10, 30]), and monolithic honeycomb (U = 150 W/m^2·K [11, 12]). A comparative lifetime analysis under the same operating conditions will measure how heat transfer coefficients that are specific to a configuration affect the formation of hotspots, the spread of deactivation waves, and the time it takes for a system to deactivate.

1.6. Thesis Objectives

The primary objective of this thesis is to extend catalyst lifetime in CO methanation by an order of magnitude, increasing their lifespan from the 45–100 hours documented by Pappagallo et al. [28] to exceed these hours, while still achieving economically viable methane yields through systematic parametric optimization and reactor configuration selection. The precise goals are as follows:

1.6.1 Comprehensive Parametric Sensitivity Analysis

Systematically investigate the effect of key operating parameters on catalyst lifetime and identify optimal operating windows, which include:

- (a) finding the best temperature to use to get the longest life while still getting $> 80\%$ CO conversion.
- (b) finding ways to manage heat to see how U and T_e affect hotspot suppression and the rate of deactivation.
- (c) finding out how pressure affects P_{tot} on the Boudouard equilibrium and reaction kinetics.
- (d) finding the best throughput, lifetime trade-offs to get the GHSV that gives the most productivity per catalyst cycle.
- (e) finding the best feed composition to get the right H_2/CO ratio and steam co-feeding effects on carbon deposition.

1.6.2 Catalyst Packing Configuration Impact Assessment

Use literature-reported total heat transfer coefficients under the same operating circumstances to compare the catalyst lifespan of the three packing configurations: standard packed bed, open-cell foam, and monolithic honeycomb. Measure how different configurations affect hotspot development, the spread of deactivation waves, and the time it takes for deactivation to happen. Determine if the increased lifespan resulting from improved heat transfer in foam (anticipated 3.6× enhancement) and monolithic (projected 2.7× enhancement) constructions warrants their elevated production costs relative to traditional packed beds.

1.7. Structure of the Thesis

The rest of this thesis is set up as follows; Chapter 2 outlines the research methodology, encompassing the comprehensive mathematical formulation of the pseudodynamic model, its implementation in MATLAB®, the utilized kinetic submodels, the kinetics of deactivation, model validation against existing literature, and the design of the parametric study. Chapter 3 presents the findings and analysis, including the detailed parametric sensitivity analysis and the comparison of catalyst packing configurations. Chapter 4 ends with a summary of the most important results, the lifetime extensions that were accomplished, the best ways to run the experiments, and suggestions for further experimental validation and model extension.

2. Methodology and Model Implementation

2.1. Overview of the Modelling Approach

This chapter presents the complete mathematical framework and computational implementation of the pseudo-dynamic model employed to simulate catalyst deactivation by coking in a fixed-bed CO methanation reactor. The model is founded on the framework originally developed by Pappagallo et al. [28], who demonstrated that the disparate time scales governing reactor phenomena permit a computationally efficient decoupling strategy. In the present thesis, this framework is extended to a substantially broader parametric space and to multiple catalyst packing configurations, thereby addressing the research gaps identified in Chapter 1.

The central premise of the pseudodynamic approach is that the chemical reactions and transport phenomena within the reactor reach a quasi-steady state on a timescale of seconds, whereas catalyst deactivation evolves over hundreds of hours. This separation of time scales, spanning roughly five orders of magnitude, permits the reactor to be modelled as proceeding through a continuous sequence of steady states, each corresponding to a progressively lower value of the local catalyst activity. The mathematical implication of this decoupling is significant: rather than resolving a system of coupled partial differential equations (PDEs) across both space and time, the issue simplifies to a solitary ordinary differential equation (ODE) in time for the catalyst activity, alongside a steady-state ODE system in the axial coordinate assessed at each deactivation time step [28].

The model structure consists of three interconnected submodels, each responsible for a distinct physical process. The steady-state reactor submodel solves the axial mass and energy balances to obtain instantaneous composition and temperature profiles at the current level of catalyst activity. The deactivation kinetic submodel evaluates the local rate of activity loss at every axial position from the current gas-phase composition and temperature. The time-integration module moves the activity profile forward in time using an explicit Euler scheme, after which a new steady-state solution is computed. This process keeps going until the outlet CO conversion drops below a critical threshold of 25%. At that point, the catalyst is said to have reached the end of its life. The model is implemented in MATLAB® with the stiff integrator `ode15s` for the steady-state reactor equations and an explicit time loop for the deactivation integration [28]. The model structure is illustrated schematically in Figure 3.

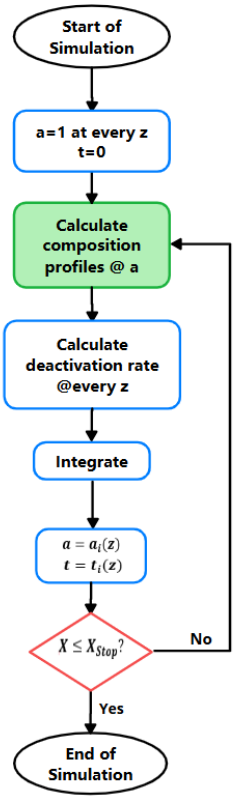

Figure 3: Pseudodynamic model structure for fixed-bed CO methanation; `X` denotes the conversion at the reactor outlet. Boxes in green refer to the reactor submodels [28].

2.2. Steady-State Fixed-Bed Reactor Submodel

2.2.1 Reactor Geometry and Operating Conditions

The reference reactor is a plate-cooled fixed-bed unit whose geometry and baseline operating conditions are taken from the pilot-scale reactor described by Moioli et al. [21] and subsequently used by Pappagallo et al. [28] for the pseudodynamic deactivation study. The reactor consists of alternating rectangular channels for reaction and cooling. The feed gas is a stoichiometric mixture for CO methanation with a H_2/CO molar ratio of 3:1. The species considered in the model are H_2, CO_2, CH_4, CO, and H_2O, indexed in this order throughout the computational implementation. In the baseline configuration, the coolant temperature T_e is set equal to the inlet gas temperature. All geometric and operating parameters are summarized in Table 3 [21, 28].

Parameter	Symbol	Value	Unit
Channel length	L	1.0	m
Channel width	W	0.50	m
Channel height (plate spacing)	h_{ch}	0.015	m
Packed-bed density	ρ_{pb}	2300	kg/m^3
Void fraction	ϵ	0.4	—
Total pressure (baseline)	P_{tot}	8	bar
GHSV (baseline)	GHSV	500	h^{-1}
H_2/CO molar ratio	—	3:1	—
Overall heat transfer coefficient	U	50	W/(m^2·K)
Inlet temperature (baseline)	T_{in}	300	°C
Coolant temperature (baseline)	T_e	$= T_{in}$	°C

Table 3: Reactor geometry and baseline operating conditions [21, 28].

Table 3 shows the geometries of the pilot-scale plate reactor operated by Moioli et al. [21] at the Paul Scherrer Institute, which was specifically designed for biogas upgrading via methanation. The plate-cooled configuration with narrow rectangular channels ($h_{ch} = 15$ mm) provides a high surface-to-volume ratio for heat removal, necessary to manage the strongly exothermic methanation reactions ($\Delta H^\circ_{298} = -206$ kJ/mol for CO methanation). The same reactor geometry was adopted by Pappagallo et al. [28], to guarantee direct comparability between this work and the reference study.

The operating pressure of 8 bar is a common industrial condition for fixed-bed methanation of synthesis gas made from biomass gasification [31]. At this pressure, the thermodynamic equilibrium strongly favors the formation of methane, which allows for almost complete conversion of CO when using a new catalyst. A GHSV of 500 h^{-1} means a medium throughput that makes sure thermodynamic equilibrium is reached within the reactor length.

The 3:1 stoichiometric H_2/CO ratio is the exact amount of CO needed for the methanation reaction. It is also the most difficult situation for coking because there is no extra hydrogen to stop the Boudouard reaction [14, 34]. The baseline inlet temperature of 300°C is the lowest value at which the methanation kinetics are fast enough to get a meaningful conversion, which is in line with the conditions used in Zhang et al.'s experiment. Coolant temperature is set equal to T_{in} in the baseline case, following the convention of Pappagallo et al. [28]; the effect of decoupling these two temperatures is investigated in Section 2.7. The overall heat transfer coefficient of 50 W/(m^2·K) is what you would expect from a normal packed bed [6, 28]. It is also the standard for comparing packing configurations in Section 2.8.

2.2.2 Governing Equations: Mass and Energy Balances

The steady-state reactor submodel is of the one-dimensional (1D) pseudo-homogeneous type [17]. The fundamental assumptions are as follows: no transport limitation exists between the gas phase and the catalyst surface or within each phase; composition and temperature gradients in the radial direction are neglected; and the gas

mixture behaves as an ideal plug flow in the axial direction. Under these assumptions, the component molar balance for species i along the axial reactor coordinate z is expressed as [28]:

$$\frac{dF_i}{dz} = \rho_{pb}(1-\epsilon)A\sum_{j=1}^{N_R} a_j(t)\nu_{ij}r_j^0 \tag{10}$$

where F_i denotes the molar flow rate of species i (kmol/s), A is the reactor cross-sectional area, ρ_{pb} is the packed-bed density, ϵ is the void fraction, $a(t,z)$ is the local catalyst activity at time t, ν_{ij} is the stoichiometric coefficient of species i in reaction j, and r_j is the rate of reaction j in kmol/(s·kg$_{cat}$). The summation extends over all $N_R = 3$ reactions considered in the kinetic submodel.
The corresponding energy balance accounts for the heat released by the exothermic reactions and the heat removed through the cooling plates [28]:

$$\frac{dT}{dz} = -\frac{\rho_{pb}(1-\epsilon)A}{\dot{m}\hat{c}_P}\sum_{j=1}^{N_R} a_j(t)\Delta h_j^R r_j - \frac{2W}{\dot{m}\hat{c}_P}U(T-T_e) \tag{11}$$

Where T is the local gas temperature (K), ΔH_j^R is the enthalpy of reaction j (J/mol), W is the channel width, U is the overall heat transfer coefficient (W/(m^2·K)), T_e is the coolant temperature (K), $\dot{m}$ is the total mass flow rate (kg/s), and $\hat{c}_P$ is the mass-specific heat capacity of the gas mixture (J/(kg·K)). The factor $2W$ comes from the fact that both sides of the rectangular reaction channel touch cooling plates. Equations 10 and 11 together make up a system of $N_C + 1 = 6$ coupled ODEs (five species plus temperature) in the spatial variable z. The initial conditions are set at $z = 0$ by the temperature and composition of the inlet.

The `ode15s` integrator in MATLAB® is used to solve the system. It is made just for stiff ODE systems. There are 150 equally spaced grid points in the spatial domain $[0, L]$. The relative and absolute tolerances are set to 10^{-6} and 10^{-8}, respectively. To make sure that the kinetic zone, where steep gradients form, has enough resolution, the maximum integration step is limited to $L/50$. The steady-state solver gets the activity profile $a(z)$ as input by using linear interpolation from a grid of $N_z = 50$ points that are evenly spaced apart.

2.2.3 Model Assumptions and Their Justification

The 1D pseudo-homogeneous reactor model relies on several simplifying assumptions whose validity determines the accuracy of the simulation results. These assumptions are discussed below, together with the physical arguments supporting their use in the present context.

Plug-flow assumption: The gas phase is considered to flow exclusively in the axial direction without back mixing. This assumption is supported by the high length-to-diameter ratio of the reactor channels ($L/h_{ch} = 1.0/0.015 \approx 67$) nd by moderate flow velocities at the baseline gas hourly space velocity (GHSV). The resulting Peclet numbers are sufficiently high, indicating that axial dispersion is negligible compared to convective transport [17].During catalyst deactivation, the plug-flow assumption remains valid because the deactivation front propagates slowly relative to the gas residence time, and axial composition gradients are primarily governed by local reaction rates rather than dispersion.

Pseudo-homogeneous assumption: The model neglects inter-phase gradients between the bulk gas and the catalyst surface, as well as intra-particle concentration and temperature gradients. This is appropriate for the relatively small catalyst particles used in methanation reactors, for which the effectiveness factor is close to unity under the operating conditions considered here. The Biot number for heat transfer within a particle is low enough that the particle can be thought of as isothermal, and the Thiele modulus is low enough that internal diffusion limits are not important [17, 28]. This simplification changes the model from a heterogeneous system of coupled gas-phase and solid-phase equations to a single set of pseudo-homogeneous balances at the reactor scale, substantially reducing the computational cost.

One-dimensional approximation: Radial gradients of temperature and composition within each channel are neglected. In the plate-cooled reactor geometry, the narrow channel height ($h_{ch} = 0.015$ m) facilitates rapid radial heat and mass transfer in comparison to axial variation. Pappagallo et al. [28] observed that the primary divergence between their model and experimental data stemmed from the challenges faced by the 1D model in accurately representing the heat-dispersing influence of the metallic reactor structure, which generally results in more uniform axial temperature profiles. This difference is minor and does not affect the prediction of the hotspot location and magnitude, which is the dominant feature governing catalyst deactivation.

Constant thermophysical properties: The gas-phase heat capacity $\hat{c}_P$ and the overall heat transfer coefficient U are treated as constant throughout the reactor. Both properties vary with temperature and composition; nevertheless, Pappagallo et al. [28] demonstrated that the model adequately represents the experimental temperature profiles using constant properties. Using constant properties also makes it easier to evaluate the sensitivity to U, since U is a single scalar parameter that can be changed on its own to compare different packing configurations (Section 2.8).

Negligible Boudouard stoichiometric effect: The stoichiometric consumption of CO by the Boudouard reaction ($2\mathrm{CO} \rightarrow \mathrm{C} + \mathrm{CO_2}$) is not accounted for in the mass balance (Equation 10). This assumption is justified by the low rate of carbon deposition compared to the main reaction rates. The Boudouard reaction only changes a small amount of the total CO flow per unit of time compared to the methanation and WGS reactions [28]. Consequently, the effect of coke formation on the gas-phase composition is negligible, and the Boudouard reaction enters the model only through the deactivation kinetic submodel (Section 2.4).

2.3. Reaction Kinetic Submodel

The kinetic submodel encompasses the three simultaneous reactions involved in CO methanation systems, as listed in Table 1 of Chapter 1. The rate expressions are derived from two independently validated experimental studies: Koschany et al. [15] for CO_2 methanation and Kopyscinski et al. [14] for CO methanation and the water–gas shift (WGS) reaction. The combination of these kinetic models has been validated against pilot-scale reactor data and adopted by Pappagallo et al. [28] as the reaction kinetic submodel for the pseudodynamic framework.

2.3.1 CO_2 Methanation (Reaction 1)

Koschany et al. [15] came up with the Langmuir–Hinshelwood–Hougen–Watson (LHHW) formalism for the rate expression for CO_2 methanation. The reference temperature is $T_{ref} = 555$ K. The rate equation considers the competitive adsorption of H_2, H_2O, and CO_2 on the catalytic surface. It also has a term that uses a thermodynamic equilibrium approach to make sure the rate goes to zero when equilibrium is reached. As Pappagallo et al. [28] say, the rate r_1 is shown as:

$$r1 = \frac{k_1 p_{H_2}^{0.5} p_{CO_2}^{0.5} \left(1 - \frac{1}{K_1^{eq}} \frac{p_{CH_4} p_{H_2O}^2}{p_{CO_2} p_{H_2}^4}\right)}{\left(1 + K_{OH,1} \frac{p_{H_2O}}{p_{H_2}^{0.5}} + \sqrt{K_{H_2} p_{H_2}} + K_{mix} p_{CO_2}^{0.5}\right)^2} \tag{12}$$

For all reactions, the kinetic constant k_j and adsorption constants K_k adhere to a modified Arrhenius equation referenced to 555 K [15]:

$$k_j = k_j^{ref} \exp\left(\frac{E_j}{R}\left(\frac{1}{T_{ref}} - \frac{1}{T}\right)\right) \tag{13}$$

$$K_k = K_k^{ref} \exp\left(\frac{\Delta h_k^{ads}}{R}\left(\frac{1}{T_{ref}} - \frac{1}{T}\right)\right) \tag{14}$$

2.3.2 Water–gas shift and CO Methanation (Reactions 2 and 3)

The kinetics of the WGS reaction and CO methanation were derived by Kopyscinski et al. [14] from spatially resolved concentration and temperature measurements in a catalytic plate reactor, using a reference temperature of $T_{ref} = 598.15$ K. Both rate expressions share a common adsorption denominator involving CO and water adsorption terms [28]:

$$r_2 = \frac{k_2 \left(K_a p_{CO} p_{H_2O} - \frac{1}{K_2^{eq}} p_{H_2} p_{CO_2}\right)}{\left(1 + K_C p_{CO}^{0.5} + K_{OH,2} \frac{p_{H_2O}}{p_{H_2}^{0.5}}\right)^2} \tag{15}$$

$$r_3 = \frac{k_3 \left(K_c \; p_{CO}^{0.5} p_{H_2}^{0.5} - \frac{1}{K_3^{eq}} p_{CH_4} p_{H_2O}\right)}{\left(1 + K_C p_{CO}^{0.5} + K_{OH,2} \frac{p_{H_2O}}{p_{H_2}^{0.5}}\right)^2} \tag{16}$$

The adsorption and kinetic constants for the Kopyscinski kinetics are also parameterized in the modified Arrhenius form of Equations 13 and 14 with $T_{ref} = 598.15$ K. The reaction enthalpies ΔH_j^R used in the implementation are as listed in Table 1 of Chapter 1.

2.3.3 Thermodynamic Equilibrium Constants

The equilibrium constants for each reaction are evaluated as functions of temperature through the following empirical correlations [28]:

$$K_1^{eq} = 137\ T^{-3.998}\ \exp\left(\frac{1.587 \times 10^5}{RT}\right) \tag{17}$$

$$K_2^{eq} = 10^{\left(2.4198 + 3.855 \times 10^{-4} T + \left(\frac{2180}{T}\right)\right)} \tag{18}$$

$$K_3^{eq} = 10^{\left(-30.42 + \frac{27106}{T}\right)} \tag{19}$$

These correlations ensure that the rate expressions in Equations 12, 15, and 16 correctly approach zero as the reaction mixture approaches thermodynamic equilibrium.

The complete set of kinetic and adsorption parameters required to evaluate Equations 12– 16 is tabulated in Appendix A (Table 8), which reproduces the parameter values reported in the Supporting Information of Pappagallo et al. [28]. In that table, activation energies and adsorption enthalpies are reported as E_j/R and $\Delta h_k^{ads}/R$ in units of Kelvin, following the convention of the sources; to recover absolute values in J/mol, one multiplies by $R = 8.314$ J/(mol·K) [28]. The equilibrium correlations of Equations 17– 19, together with the parameters in Appendix A, enable full reproduction of all simulation results presented in this thesis.

2.4. Deactivation Kinetic Submodel

2.4.1 Definition of Catalyst Activity

The catalyst activity a is defined as the ratio of the current reaction rate on a partially deactivated catalyst to the rate that would be observed under identical conditions on a fresh catalyst [28]:

$$a = \frac{r_j}{r_j^0} \tag{20}$$

Where r_j^0 denotes the rate on a fresh catalyst [28]. Since CO methanation is assumed to be perfectly selective toward methane production [28], a single activity variable a is used for all three reactions. The activity is bounded between 0 (completely deactivated) and 1 (fresh catalyst). In the reactor submodel, every reaction rate is multiplied by the local value of $a(z,t)$, as shown in Equations 10 and 11.

2.4.2 Deactivation Rate Equation and Calibration

The rate of catalyst deactivation follows a semi-empirical power-law formulation adapted from Sun et al. [32] and parameterized by Pappagallo et al. [28] for CO methanation using the experimental data of Zhang et al. [34]. The global deactivation model is expressed as [28]:

$$\frac{da_j}{dt} = -r_{d,j} \cdot a_j^{\beta} \tag{21}$$

$$r_{d,j} = k_{d,j} \cdot p_{CO}^{\alpha} \cdot f_{H_2O} \tag{22}$$

Where p_{CO} is the local partial pressure of CO, f_{H_2O} is a correction factor accounting for the inhibiting effect of water on carbon deposition, and $k_{d,j}$ is the temperature-dependent deactivation rate constant following an Arrhenius relationship:

$$k_{d,j} = k_{d,j}^0 \cdot \exp\left(-\frac{E_{d,j}}{RT}\right) \tag{23}$$

The water correction factor is formulated as an empirical function that decreases the deactivation rate with increasing local water mole fraction x_{H_2O} [28]:

$$f_{H_2O} = \frac{x_{H_2O} - 1}{(1 - c) \cdot x_{H_2O} - 1} \tag{24}$$

Where c is the correction intensity parameter (Table 4), this factor ranges from approximately unity near the reactor inlet, where no water has yet been produced, to values approaching zero at high water contents near the outlet [28]. The physical interpretation is that water kinetically inhibits coke formation on active sites by competing for adsorption or by partially gasifying carbon precursors [28]. It is important to emphasize that this correction captures a kinetic inhibition effect operating at all temperatures and does not represent the thermodynamic regeneration of coked catalysts via steam gasification, which requires temperatures above 400°C [28, 31].

Pappagallo et al. [28] used regression on the experimental data published by Zhang et al. [34] to find the deactivation parameters. Zhang et al. [34] measured how long it took for CO to change from one state to another in a laboratory-scale fixed-bed reactor at three different temperatures between 320 and 360°C. The fitting procedure employed a simplified activity definition $a_r = X/X_0$ [28], where X is the outlet CO conversion and X_0 its initial value. The resulting parameter set is listed in Table 4.

Symbol	Parameter	Value	Unit
$k^0_{d,j}$	Pre-exponential factor	0.182	—
$E_{d,j}$	Activation energy	48,418	J/mol
α	Reaction order (CO)	1	—
c	Correction intensity	0.01	—
β	Activity influence parameter	1	—

Table 4: Deactivation kinetic parameters calibrated from Zhang et al. [34] data [28].

The first-order activity dependence ($\beta = 1$) implies that the deactivation rate is directly proportional to the remaining activity, with an approximate exponential decay under constant conditions, comparable with frequently noted coking behavior [28]. The activation energy reflects the high temperature sensitivity of the Boudouard reaction; a hotspot-scale temperature increase (approximately 70°C above the bulk bed temperature) will increase the rate of local deactivation by a factor of 30–50 [28].

2.5. Pseudodynamic Model: Coupling of Submodels

2.5.1 Time-Scale Separation and Model Structure

The pseudodynamic model is the principal methodological innovation of the reference framework [28]. Its name reflects the fact that it achieves dynamic modelling of the reactor performance over the deactivation time scale (hours) without resorting to partial differential equations. The key assumption is that at any instant during the deactivation process, the reactor can be treated as operating at steady state because the reaction and transport time scales (seconds) are negligibly short compared to the deactivation time scale (hours). The model ODE is therefore simply:

$$\frac{da(z)}{dt} = -r_d(z) \cdot a(z)^{\beta} \tag{25}$$

Where the local deactivation rate $r_d(z)$ depends on the local partial pressure of CO and the local temperature, both of which are outputs of the steady-state reactor solved at the current activity profile. In the fixed-bed case, the activity is not a single scalar but a profile, $a(z, t)$ that evolves independently at each axial position according to the local gas-phase composition and temperature. This spatial dependence is fundamental: it captures the formation of the deactivation wave, whereby the catalyst in the inlet kinetic zone (high CO partial pressure and high hotspot temperature) deactivates first, and the reaction front progressively migrates downstream [28].

2.5.2 Computational Algorithm

The pseudodynamic model is implemented as an explicit time-integration loop with $N_t = 100$ uniformly spaced time steps over the simulation horizon $[0, t_{max}]$. At each time step, the following sequence of operations is

executed:

- **Step 1 – Steady-state reactor solve.** Given the current activity profile $a(z)$, the steady-state reactor submodel (Section 2.2) is called to compute the axial profiles of molar flow rates $F_i(z)$, temperature $T(z)$, CO conversion $X_{CO}(z)$, and mole fractions $y_i(z)$.

- **Step 2 – Deactivation rate evaluation.** At each of the $N_z = 50$ axial grid points, the local CO partial pressure $p_{CO}(z) = P_{tot} \cdot y_{CO}(z)$, the local temperature $T(z)$, and the water mole fraction $x_{H_2O}(z)$ are extracted from the steady-state solution. The deactivation rate $r_d(z)$ is then computed from Equations 22– 24.

- **Step 3 – Activity update.** Advance the activity profile in time using the explicit (forward) Euler scheme: $a(z, t + \Delta t) = a(z, t) + \left(\frac{da}{dt}\right) \cdot \Delta t$, where $\frac{da}{dt} = -r_d(z) \cdot a(z, t)^\beta$ from Equation 25. Clamp the updated activity to the interval $[0, 1]$.

- **Step 4 – Termination check.** End the simulation when the outlet CO conversion $X_{CO}(z = L)$ falls below 0.25, indicating the catalyst has reached the end of its life.

For every time step, this four-step cycle is repeated. The repeated steady-state reactor solves (Step 1) predominate the computational cost, each of which requires a single call to the MATLAB® `ode15s` integrator. Since every such call involves only a six-dimensional ODE system over a one-dimensional spatial domain, for a complete deactivation simulation (100–2000 hours of simulated time), the total wall-clock time is on the order of tens of seconds on a standard workstation. This computational efficiency gives it an important advantage, the pseudodynamic approach, since it allows the extensive parametric sweeps described in Section 2.7.

2.5.3 Numerical Considerations

The explicit Euler scheme used for the temporal integration of the activity profile introduces a constraint on the maximum allowable time step to ensure numerical stability. For the first-order activity dependence ($\beta = 1$), the activity update at each axial position takes the form $a_{new} = a_{old} \cdot (1 - r_d \cdot \Delta t)$. For the scheme to remain stable, the product $r_d \cdot \Delta t$ must be less than unity at every grid point. The maximum deactivation rate occurs at the hotspot, where both the temperature and the CO partial pressure are highest. Under the most aggressive conditions considered in this study ($T_{in} = 450$°C, adiabatic-like operation), the hotspot deactivation rate can reach approximately 10^{-3} h^{-1}, implying a stability limit of $\Delta t < 1000$ h. Since the simulation horizon is at most 130 h for the fixed bed and the number of time steps is $N_t = 100$, the resulting $\Delta t \approx 1.3$ h is well within the stability limit for all cases investigated.

The spatial discretization of the activity profile on an $N_z = 50$ grid points has been verified to provide grid-independent results. Preliminary convergence tests at the baseline conditions showed that doubling the number of grid points to $N_z = 100$ changed the predicted time-to-25%-conversion by less than 2%, confirming that 50 points are sufficient to resolve the deactivation wave. The steady-state reactor solver uses a finer internal grid of 150 points (controlled by `ode15s`) to resolve the steep temperature and concentration gradients in the kinetic zone, and the solution is subsequently interpolated onto the coarser deactivation grid.

The coupling between the spatial ODE (steady-state reactor) and the temporal ODE (activity evolution) is handled explicitly, meaning that the activity is frozen during each steady-state solve and updated only between solves. This sequential coupling is justified by the time-scale separation: the composition and temperature profiles adjust instantaneously (relative to the deactivation time scale) to any change in the activity profile. The accuracy of this one-way coupling has been confirmed by Pappagallo et al. [28], who showed that the pseudodynamic approach reproduces the expected deactivation wave dynamics and matches experimental time-on-stream data.

2.6. Model Validation

The full pseudodynamic model is validated by reproducing the key results reported by Pappagallo et al. [28] for the fixed-bed CO methanation case. The steady-state reactor submodel was originally validated by Pappagallo et al. [28] against pilot-scale experimental temperature profiles from Moioli et al. [21], showing good agreement for hotspot location and magnitude. The deactivation kinetic submodel was calibrated against the time-on-stream data of Zhang et al. [34] at 320, 340, and 360°C [28], confirming the Arrhenius consistency of the parameterization.

In the present work, the complete pseudodynamic model is benchmarked by verifying that it reproduces:

- **Fresh-catalyst conversion and temperature profiles**: showing the characteristic three-zone structure (kinetic zone, heat-transfer-controlled zone, and thermodynamic zone).
- **Deactivation wave propagation**: the wave of deactivation that forms and spreads over time.
- **Thermal hotspot migration**: the migration of the thermal hotspot along the reactor axis as deactivation progresses.
- **Catalyst lifetime**: the time for 25% the time-to-25%-conversion at inlet temperatures between 300°C and 360°C [28].

Successful reproduction of these benchmarks proves that the implementation is correct and consistent. It also sets the standard for all parametric changes and configuration comparisons.

2.7. Design of Parametric Study

The parametric investigation in this thesis substantially extends the parameter space explored by Pappagallo et al. [28], who limited their analysis to four inlet temperatures between 300 and 360°C at a single pressure, space velocity, and heat transfer coefficient. In the present work, seven operating parameters are varied systematically across industrially relevant ranges, as summarized in Table 5. Each parameter is varied individually while keeping all other parameters at their baseline values, yielding a one-at-a-time (OAT) sensitivity analysis.

Symbol	Parameter	Baseline	Range	Physical Rationale
T_{in}	Inlet temperature [°C]	300	250–450	Kinetic control to equilibrium limit
T_e	Coolant temperature [°C]	$= T_{in}$	200–400	Coolant decoupled from inlet
U	Heat transfer coeff. [W/(m²·K)]	50	10–1000	Natural conv. to active exchange
P_{tot}	Total pressure [bar]	8	5–20	Industrial methanation range
$GHSV$	GHSV [h^{-1}]	500	500–25,000	Low to high throughput
H_2/CO	Molar ratio	3	1–5	Sub-stoichiometric to excess H_2
Steam	Steam fraction [%]	0	0–20	Co-feeding for coking suppression

Table 5: Operating parameter ranges for parametric sensitivity analysis.

The rationale for each parameter range is summarized in the rightmost column of Table 5. The seven parameters can be grouped into three categories according to their role in the reactor system, which also motivates the structure of the results discussion in Chapter 3.

- **Thermal management parameters**: Includes T_{in}, T_e, and U. Together, these variables determine the temperature profile and the magnitude/location of the thermal hotspot. Since deactivation kinetics follow an Arrhenius law (Equation 23), the temperature profile is the most direct lever on catalyst lifetime. This study decouples T_e from T_{in} to explore sub-cooling, whereas the reference study maintained $T_e = T_{in}$ [28].

- **Composition and residence time parameters**: Include total pressure P_{tot} and gas hourly space velocity $GHSV$. Partial pressures influence both methanation kinetics and Boudouard equilibrium, whereas $GHSV$ controls the reactive zone extent and gas residence time.

- **Feed composition parameters**: Covers the H_2/CO molar ratio and the steam fraction. Both directly affect CO and H_2O concentrations in the deactivation rate expression (Equation 22) and its water correction factor (Equation 24). Sub-stoichiometric ($H_2/CO < 3$) and dry feeds represent aggressive conditions for carbon deposition [32].

2.7.1 Performance Metrics

For each simulation case, two time-evolution curves are recorded as the principal outputs: the outlet CO conversion and the spatially averaged catalyst activity. Each parametric variation in Table 5 produces a family of these curves, from which the sensitivity of reactor performance to the varied parameter can be directly assessed.

The conversion curve reflects the global reactor output visible to a process operator, while the activity curve reveals the internal state of the catalyst bed.

The main measure of performance in this study is the time-to-25%-conversion (t_{25}), which is the time on stream until the CO conversion at the reactor outlet goes below the 25% threshold. Pappagallo et al. [28] introduced this metric as a practical indicator of catalyst end of life, below which reactor output is no longer considered economically viable for synthetic natural gas (SNG) production. In addition to t_{25}, several secondary metrics are evaluated:

- **Fresh-catalyst conversion ($X_{CO,0}$)**: The outlet CO conversion on a fresh catalyst ($t = 0$), quantifying initial reactor performance. Although a higher $X_{CO,0}$ is generally desirable, it may result in a larger hotspot and consequently faster deactivation.

- **Peak hotspot temperature (T_{max})**: Refers to the maximum temperature in the reactor at $t = 0$ and serve as a key indicator of the thermal stress on the catalyst. Given that deactivation kinetics follow Arrhenius behavior, the hotspot temperature is the most significant factor controlling the local deactivation rate. A reduction in T_{max} directly extends catalyst lifetime.

- **Deactivation wave velocity**: The speed at which the deactivation front propagates through the reactor is a qualitative indicator of the spatial distribution of deactivation. A slower wave velocity implies that the catalyst bed maintains its performance for a longer time. This metric is extracted from the spatiotemporal activity profiles $a(z, t)$.

2.7.2 Expected Parameter Interactions

The parametric study uses a one-at-a-time (OAT) method, but we can expect some interactions between the parameters based on what we know about physics. These interactions will help us understand the results. The inlet temperature T_{in} interacts strongly with the heat transfer coefficient U; at low U, T_{in} has only a small effect on the hotspot temperature because the exothermic heat release is the main factor in the energy balance, whereas at high U, the coolant temperature T_e becomes the primary determinant of the bed temperature. Similarly, the total pressure P_{tot} has affect on the both the forward reaction rate (favoring higher conversion) and the Boudouard equilibrium (favoring carbon deposition), creating a non-monotonic dependence of catalyst lifetime on pressure.

The $GHSV$ interaction with the deactivation wave dynamics: a higher space velocity shifts the reaction zone toward the outlet of the reactor, which may delay the start of conversion loss even as it reduces the initial conversion. The H_2/CO ratio has a direct effect on the CO partial pressure in the kinetic zone, with sub-stoichiometric feeds ($H_2/CO < 3$) increasing p_{CO} and thus the deactivation rate according to Equation 22, while excess hydrogen speeds up CO consumption and reduces the reactive zone. Finally, steam co-feeding at the same time dilutes the CO partial pressure and raises the water correction factor f_{H_2O} (Equation 24), producing a synergistic suppression of deactivation. These expected interactions are extensively analyzed in the results presented in Chapter 3.

2.8. Catalyst Packing Configuration Comparison

The second stage of the research methodology addresses Gap 2 identified in Chapter 1: the absence of a comparative assessment of catalyst lifetime across different packing configurations under identical methanation conditions. The fundamental hypothesis is that enhanced heat transfer, achieved through structured catalyst supports (foams and monoliths), suppresses the thermal hotspot and thereby reduces the local deactivation rate according to the Arrhenius dependence of the Boudouard kinetics.

2.8.1 Physical Description of the Packing Configurations

The three catalyst packing configurations considered in this study differ in their internal structure, which directly determines the heat transfer characteristics within the reactor. Their physical properties and literature context were reviewed in Section 1.3.6 of Chapter 1; only the features relevant to the modelling approach are summarized here.

- **Conventional packed bed**: The baseline configuration consists of randomly packed catalyst pellets. Heat is transferred through a combination of inter-particle conduction, gas-film conduction, and intersti-

tial convection. The tortuous flow path creates local stagnation zones where heat removal is inefficient, resulting in a pronounced thermal hotspot in the kinetic zone. This configuration represents the reactor studied experimentally by Pappagallo et al. [28] and validated in Section 2.6.

- **Monolithic honeycomb**: A ceramic or metallic structure with parallel channels (1–3 mm in diameter) coated with a thin layer of catalyst washcoat. The continuous solid matrix creates a direct conduction path from the reaction zone to the cooling plwhich is significantly more efficient than the point-contact conduction in packed beds. The laminar flow and thin catalyst layer also minimize interparticle diffusion limitations.

- **Open-cell foam**: An open-cell metallic or ceramic foam (70–95% porosity) coated with an active catalyst. The three-dimensional strut network makes it possible for conduction paths in all directions, while the open-cell structure promotes turbulent flow even at low velocities. This combination yields the highest effective thermal conductivity of the three configurations.

2.8.2 Modelling Strategy for Configuration Comparison

The same pseudodynamic framework is used to model the three different catalyst packing configurations; the only thing that changes is the overall heat transfer coefficient U in Equation 11. The geometry, feed composition, pressure, GHSV, and reactor kinetics remain the same. This approach isolates the effect of heat transfer enhancement on deactivation and enables a direct comparison of catalyst lifetimes. From Table 2, we get the U values for each configuration: 50 W/(m^2·K) for the packed bed, 150 W/(m^2·K) for the monolithic honeycomb, and 250 W/(m^2·K) for the open-cell foam, where the literature sources and selection reasons are discussed in detail (Section 1.3.6). These values represent conservative mid-range estimates from the cited sources, ensuring that the predicted lifetime improvements can be made with current commercial technology and give a lower-bound estimate of the benefits of structured catalysts.

2.8.3 Expected Physical Effects of Enhanced Heat Transfer

The enhanced heat removal in foam and monolithic configurations produces two synergistic effects that reduce catalyst deactivation. Firstly, a higher U value reduces the magnitude of the thermal hotspot by more efficiently transferring the heat generated in the kinetic zone to the cooling medium. The Arrhenius temperature dependence of the deactivation kinetics (Equation 23) means that even modest hotspot reductions translate into large decreases in the local deactivation rate. For instance, reducing the peak temperature from 612°C (packed bed) to 539°C (foam) corresponds to a factor of approximately 30–50 decrease in the local deactivation rate at the hotspot location, based on the activation energy of 48,418 J/mol [28].

Secondly, a more uniform temperature profile leads to a broader and less concentrated reaction zone, which distributes the deactivation more evenly across the catalyst bed. In a packed bed, the sharp hotspot causes rapid localized deactivation that creates a well-defined deactivation wave propagating downstream. In a foam or monolith reactor, the broader temperature profile is expected to produce a more diffuse deactivation front, which delays the onset of conversion loss at the reactor outlet. These predictions, derived from the Arrhenius sensitivity analysis, are consistent with the experimental observations of Richardson et al. [30], who reported hotspot reductions of 100–200°C for ceramic foams, and Groppi and Tronconi [11], who reported 50–100°C reductions for monolith reactors in exothermic applications.

2.9. Computational Implementation in MATLAB®

The full model is built in MATLAB® and consists of four interconnected scripts and function files. The main driver script runs both parametric studies and configuration comparison, calls the reactor and deactivation functions, and generates all output plots. A dedicated steady-state reactor function receives the inlet conditions, operating parameters, and an activity profile as inputs and returns the axial profiles of molar flows, temperature, CO conversion, and mole fractions. A separate kinetics function calculates the three reaction rates and the total heat release at any given local partial pressures and temperature; it is fully vectorized to enable efficient batch evaluation. The pseudodynamic time-loop function applies explicit Euler time integration described in Section 2.5.2, calling the reactor solver at each time step and updating the activity profile.

The MATLAB® code structure has been designed for modularity and extensibility. Each submodel is encapsulated in a separate function, which facilitates independent testing, validation, and future refinement. The use of the stiff integrator `ode15s` for the spatial ODE ensures numerical stability in the kinetic zone where steep

temperature gradients develop. The explicit Euler scheme for the temporal integration is justified by the slow evolution of the activity profile, which ensures that the time step Δt (typically on the order of 1–2 hours) is sufficiently small relative to the deactivation time scale. For the parametric study, the main script executes a loop over the parameter values specified in Table 2, generating a complete deactivation simulation for each case. The output for each case includes:

- **Time-on-stream evolution**: Outlet CO conversion and average activity.
- **Spatiotemporal profiles**: Axial profiles over time for activity, temperature, and conversion.
- **Performance metrics**: Specifically t_{25}, T_{max}, and $X_{CO,0}$.

These outputs are stored in structured arrays for subsequent visualization and comparison.

2.10. Chapter Summary

This chapter presentes the complete methodology developed for simulating deactivation by coking in a fixed-bed CO methanation reactor. The approach is built on the pseudodynamic framework introduced by Pappagallo et al. [28], in which the large separation between the time scales of reaction (seconds) and deactivation (hundreds of hours) is exploited to model the reactor as proceeding through a sequence of steady states at progressively decreasing catalyst activity.

The mathematical model consists of four interconnected components:

- **Steady-state reactor submodel** (Section 2.2): This submodel solves one-dimensional mass and energy balances in a plate-cooled geometry validated against pilot-scale data (Section 2.6).
- **Reaction kinetic submodel** (Section 2.3): Employs three LHHW rate expressions for CO_2 methanation, the water–gas shift, and CO methanation, with parameters drawn from the literature of Koschany et al. [15] and Kopyscinski et al. [14].
- **Deactivation kinetic submodel** (Section 2.4): Application of a power-law formulation calibrated against the experimental data of Zhang et al. [34], with CO partial pressure as the primary driving force and a water correction factor representing the inhibiting effect of steam on coke formation.
- **Pseudodynamic time-integration module** (Section 2.5): Combines these submodels through an explicit Euler scheme which facilitates the propagation of the spatially resolved activity profile in time.

Two different ways to apply the model are explored in the current study. The first is a one-at-a-time parametric sensitivity analysis (Section 2.7) covering seven operating parameters—inlet temperature, coolant temperature, heat transfer coefficient, total pressure, space velocity, H_2/CO ratio, and steam fraction to identify the conditions that maximize catalyst lifetime. The second is a comparative evaluation of three catalyst packing configurations (Section 3.4)—packed bed, monolithic honeycomb, and open-cell foam—modelled through their characteristic heat transfer coefficients.

Findings of these inquiries are discussed in Chapter 3. It starts with deactivation behavior at the reference conditions in Table 3, such as the deactivation wave structure and the moving hotspot effect. The parametric sensitivity results are further analyzed parameter-wise, taking into consideration the trade-off between initial conversion and catalyst lifetime. Finally, the packing configuration comparison quantifies the lifetime extension achievable through enhanced heat transfer.

3. Results and Discussion

3.1. Introduction

This chapter presents the simulation results obtained from the pseudodynamic model described in Chapter 2. The analysis is organized in three stages of increasing scope, each building on the findings of the preceding one. Section 3.2 establishes the baseline deactivation behavior at the reference conditions of Table 3, documenting the spatiotemporal evolution of catalyst activity, temperature, and CO conversion. Section 3.3 presents the results of the one-at-a-time parametric sensitivity analysis across the seven operating parameters defined in Table 5. Section 3.4 compares the performance of the three catalyst packing configurations—packed bed, monolithic honeycomb, and open-cell foam—through their characteristic heat transfer coefficients, as described in Section 3.4. Section 3.5 synthesizes the findings by ranking the parameters according to their impact on catalyst lifetime and identifying the operating windows that offer the greatest potential for lifetime extension.

Throughout this chapter, the primary performance metric is the time-to-25%-conversion, t_{25}, defined in Section 2.7.1 as the number of hours on stream at which the outlet CO conversion drops below 25%. This threshold was adopted from Pappagallo et al. (2025) [28] as a practical end-of-life criterion for industrial SNG production. Supporting metrics include the fresh-catalyst conversion $X_{CO,0}$, the peak hotspot temperature T_{max}, and the spatially averaged catalyst activity $\bar{a}(t)$. All figures referenced in this chapter correspond to MATLAB®-generated plots from the simulation framework described in Section 2.9.

3.2. Behavior of baseline Deactivation

The baseline simulation takes place under the conditions listed in Table 3: $T_{in} = 300$°C, $P_{tot} = 8$ bar, $GHSV = 500$ h^{-1}, $H_2/CO = 3{:}1$ (stoichiometric), $U = 50$ W/(m^2·K), and $T_e = T_{in}$. This section describes the three key aspects of the spatiotemporal evolution: the fresh-catalyst profiles, the deactivation wave, and the moving hotspot.

3.2.1 Fresh-Catalyst Profiles

The axial profiles of CO conversion and temperature on the fresh catalyst ($a(z) = 1$ everywhere) are shown in Figure 4 for inlet temperatures of 300, 320, 340, and 360°C. These profiles establish the initial condition from which deactivation proceeds and serve as the benchmark for measuring the subsequent performance loss.

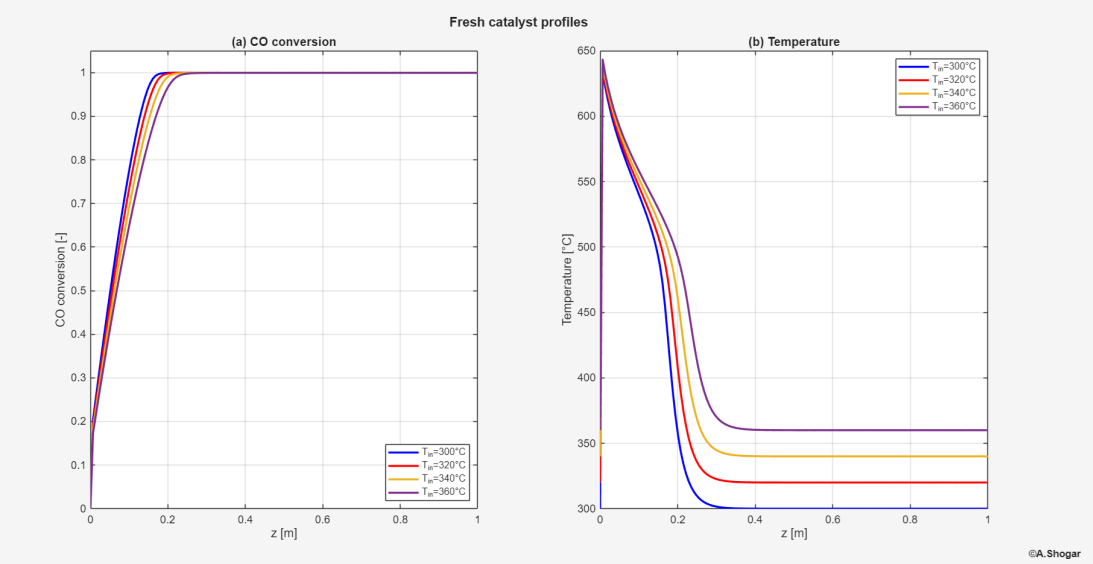

Figure 4: Fresh catalyst axial profiles: (a) CO conversion and (b) temperature at four different inlet temperatures (300–360°C). Conditions: P = 8 bar, GHSV = 500 h^{-1}, $H_2/CO = 3{:}1$.

Three distinct zones are identifiable in each profile, consistent with the description by [28]. The first 5–10 cm constitutes the kinetic zone, characterized by a high concentration of reactants that drives a rapid reaction rate, a steep increase in CO conversion, and an intense release of reaction heat. At $T_{in} = 300$°C, the temperature rises

sharply to a peak of approximately 620°C within this zone, forming the thermal hotspot. The CO conversion reaches approximately 30% in this narrow region.

The next 10–20 cm is the heat-transfer dependent zone. As the reactants are depleted progressively, they tend to decrease the reaction rate, and the cooling system starts to dominate the energy balance, drawing the temperature back down to the coolant level. The conversion continues to increase, at a much slower rate and close to the maximum thermodynamic equilibrium limit. By $z \approx 0.20$ m at 300°C, the conversion has effectively reached unity. The rest of the reactor constitutes the thermodynamic zone where the equilibrium has been reached, and no further net reaction occurs. The transition from one state to another has been obtained at all four inlet temperatures, and at each of these times equilibrium conversion is greater than 99%; thus, the outlet conversion is effectively 100%.

Increasing the inlet temperature from 300 to 360°C has two competing effects: it speeds up the kinetics, shrinking the kinetic zone from approximately $z \approx 0.20$ m to $z \approx 0.12$ m, and it increases the hotspot temperature. At $T_{in} = 360$°C, the maximum temperature reaches approximately 648°C, nearly 30°C above the 300°C case. The downstream asymptotic temperatures also differ, settling at approximately 300, 325, 340, and 365°C for the respective inlet temperatures, reflecting the coolant temperature ($T_e = T_{in}$). This observation is crucial for the deactivation analysis because the Boudouard reaction rate follows an Arrhenius dependence (Equation 23), meaning that the 320°C temperature rise from the inlet to the hotspot under baseline conditions accelerates the local deactivation rate by orders of magnitude faster than that of the inlet value.

3.2.2 Deactivation Wave Propagation

Figure 5 shows the spatiotemporal evolution of the catalyst activity profile $a(z,t)$ and the resulting CO conversion profile $X_{CO}(z,t)$ at $T_{in} = 300$°C, plotted at 10-hour intervals from $t = 0$ to the point at which the outlet conversion drops below 25%.

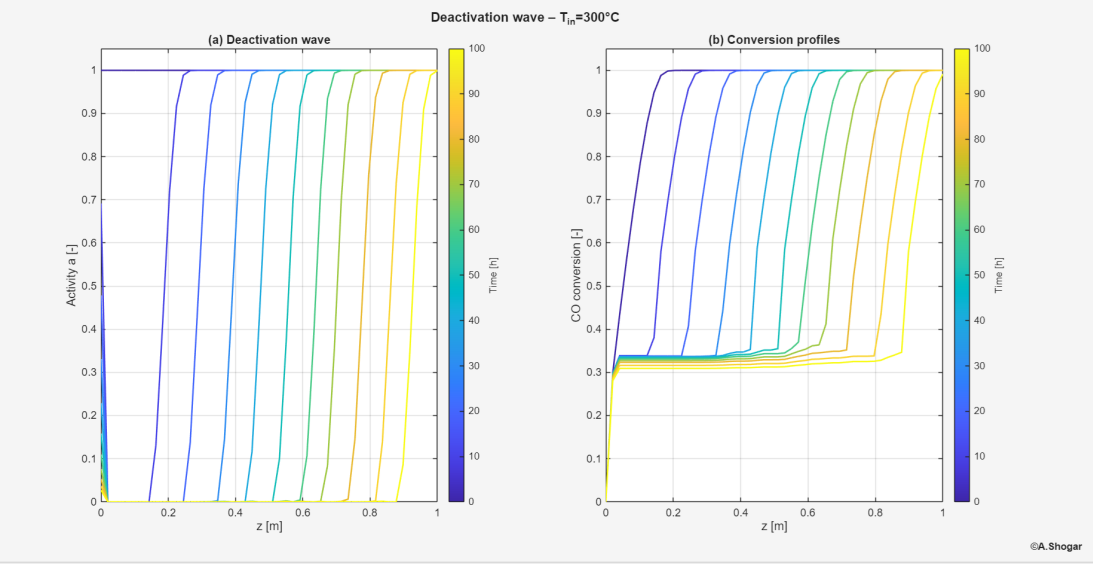

Figure 5: Deactivation wave at $T_{in} = 300$°C: (a) Activity profile $a(z,t)$ and (b) CO conversion profile $X_{CO}(z,t)$ are shown at 10-hour intervals.

At $t = 0$, the activity is uniformly equal to unity across the reactor. Over time, a clear deactivation front forms near the reactor inlet. This is where the CO partial pressure is highest and the spot temperature is highest, which leads to the fastest coke deposition. By $t = 10$ h, the activity in the first 5–10 cm drops to almost zero, but the rest of the bed stays near-unity activity. This localized loss of activity transforms the original kinetic zone into an inactive zone where no appreciable reaction occurs.

As the inlet portion of the catalyst bed loses activity, the region of high reactant concentration, therefore, high reaction rate shifts downstream. A new kinetic zone forms in the adjacent section of the bed where the catalyst is still active, and the gas is still rich in CO. This downstream migration of the reaction front creates the characteristic "deactivation wave" described by Pappagallo [28]. The wave advances steadily toward the reactor outlet, consuming active catalyst as it moves. The front has moved to $z \approx 0.40$–0.50 m (the midpoint of the bed) by $t \approx 50$ h and to $z \approx 0.80$–0.90 m, getting closer to the reactor outlet, by $t \approx 100$ h.

The deactivation front is very sharp because the temperature and deactivation rate work together to make it that way. The exothermic reaction in the kinetic zone raises the local temperature, which makes the Boudouard coking rate rise exponentially through the Arrhenius term (Equation 23). The faster coking destroys the local catalyst activity, which extinguishes the reaction and causes it to shift downstream. This self-reinforcing mechanism produces a front that is only a few centimeters wide, separating a completely inactive upstream region ($a \approx 0$) from a still-active downstream region ($a \approx 1$). The front velocity depends on the local deactivation rate, which in turn depends on the hotspot temperature and the CO partial pressure, both of which are determined by the position within the reactor.

The practical effect of this wave-like phenomenon is that the outlet conversion is maintained for an extended period, only to drop off sharply once the front arrives in the thermodynamic zone. From an operational perspective, this means that a conventional conversion-based monitoring methodology would catch this deactivation only after a significant fraction of the catalyst bed has been irreversibly degraded. A temperature-based monitoring approach, which tracks the position and magnitude of the hotspot, would provide an earlier and more useful picture of the deactivation progress.

A critical observation from Figure 5(b), the outlet CO conversion is practically unchanged (near 100%) for the first approximately 50–60 hours of operation. The deactivation wave is still in the heat-transfer-controlled zone, and the thermodynamic zone, where the equilibrium conversion has been reached, extends all the way to the outlet. Only when the deactivation front passes $z \approx 0.60$ m does the outlet conversion begin to decline. Once the decline begins, it progresses fast: the conversion profiles show a typical plateau at $X_{CO} \approx 0.30$–0.35 corresponding to the output of the narrow kinetic zone only (the heat-transfer-controlled and thermodynamic zones are taken away), and the 25% threshold is reached at approximately $t_{25} \approx 100$ h in the above baseline situations.

3.2.3 Moving Hotspot Phenomenon

Figure 6 presents the axial temperature profiles at 10-hour intervals, illustrating the downstream migration of the thermal hotspot.

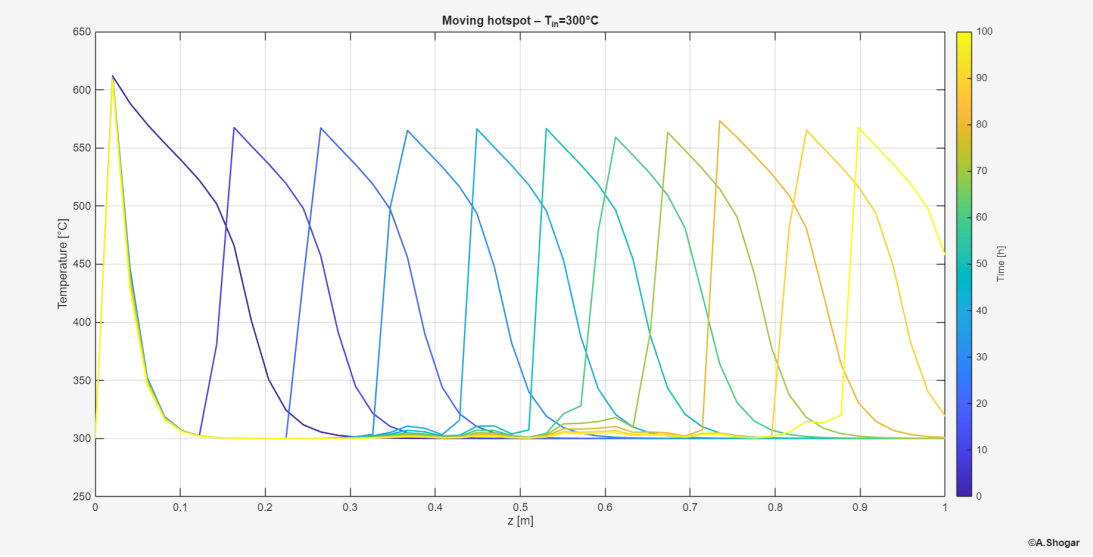

Figure 6: Moving hotspot at $T_{in} = 300$°C: axial temperature profiles at 10-hour intervals.

At $t = 0$, the hotspot is located near the reactor inlet ($z \approx 0.02$–0.03 m), corresponding to the kinetic zone, with a peak temperature of approximately 612°C. As the catalyst in this region deactivates, the exothermic reaction stops happening there, and the hotspot then moves downstream to the new kinetic zone, where the catalyst is still working, and the gas is still rich in CO. The peak has moved to $z \approx 0.20$ m by $t \approx 20$ h and to $z \approx 0.45$–0.50 m by $t \approx 50$ h. The hotspot has moved to $z \approx 0.75$–0.80 m by $t \approx 80$ h, and it has moved to $z \approx 0.90$–0.95 m by $t \approx 100$ h, approaching the reactor outlet.

A notable feature visible in Figure 6 is that the hotspot magnitude decreases as it migrates downstream. The initial hotspot at $t = 0$ reaches approximately 612°C, while the migrating peaks stabilize at approximately 565–575°C for $t = 20$–70 h. As the front approaches the outlet ($t > 80$ h), the peak temperature decreases further

to approximately 460–500°C because the reaction front is running out of bed length: the remaining catalyst volume is insufficient to sustain the full reaction, the gas has less residence time to react, and the cooling system continues to extract heat. Behind each hotspot, the temperature returns to approximately 300°C (the coolant temperature), confirming that the deactivated upstream section is thermally inert.

The downstream migration of the hotspot has two important physical consequences. First, it subjects progressively deeper sections of the catalyst bed to the elevated thermal stress that accelerates Boudouard coking. Second, the decreasing hotspot magnitude as the front advances means that the local deactivation rate actually slows as the wave moves downstream, which is why the front velocity is not constant but gradually decreases over time. This self-decelerating behavior explains why the conversion at the outlet remains high for an extended period before dropping relatively abruptly once the deactivation front reaches the final section of the bed.

The downstream migration of the hotspot is intrinsically connected to the deactivation wave; both are coupled manifestations of the same underlying process. The hotspot's position at any given time serves as a direct visual indicator of the deactivation front's progression through the bed and marks the location of the highest local deactivation rate at each moment.

3.2.4 Baseline Performance Summary

Table 6 summarizes the key performance metrics at the baseline condition and at three additional inlet temperatures, establishing the reference values against which all parametric variations will be compared.

Table 6: Baseline performance metrics at four inlet temperatures.

Metric	**300°C**	**320°C**	**340°C**	**360°C**
$X_{CO,0}$ [%]	100	100	100	100
T_{max} [°C]	≈ 620	≈ 630	≈ 640	≈ 648
Plateau duration [h]	≈ 80	≈ 65	≈ 45	≈ 30
t_{25} [h]	≈ 120	≈ 100	≈ 78	≈ 52
Hotspot location at $t = 0$ [m]	0.02–0.03	0.02–0.03	0.01–0.02	0.01–0.02

The results in Table 6 reveal a clear trade-off: increasing T_{in} from 300 to 360°C raises the hotspot temperature by approximately 28°C and reduces the catalyst lifetime t_{25} from approximately 120 h to approximately 52 h, a 57% reduction [28]. The fresh-catalyst conversion $X_{CO,0}$ is 100% in all four cases because the $GHSV$ is sufficiently low to allow thermodynamic equilibrium to be reached. The conversion plateau—the period during which the outlet conversion remains at 100%—shrinks from 80 h to 30 h over the same temperature range. These baseline values are consistent with the findings of Pappagallo [28], who reported t_{25} values of 45–100 h under similar operating conditions.

3.3. Parametric Sensitivity Analysis

This section presents the results of the one-at-a-time (OAT) parametric sensitivity analysis across the seven operating parameters defined in Table 2.4. For each parameter, the time-evolution of the outlet CO conversion $X_{CO}(t)$ and the spatially averaged activity $\bar{a}(t)$ are presented, and the resulting t_{25} values are compared. The parameters are organized into three groups, following the structure established in Section 2.7: thermal management (Section 3.3.1–3.3.3), operating conditions (Section 3.3.4–3.3.5), and feed composition (Section 3.3.6–3.3.7).

3.3.1 Effect of Inlet Temperature (T_{in})

Figure 7 shows the time-evolution of outlet CO conversion and average catalyst activity for inlet temperatures of 300, 320, 340, and 360°C. All four cases achieve an initial conversion of 100%, confirming that the baseline $GHSV$ is sufficiently low for thermodynamic equilibrium to be reached on the fresh catalyst. The conversion remains at this plateau for a duration that depends strongly on T_{in}: approximately 80 h at 300°C, 65 h at 320°C, 45 h at 340°C, and only 30 h at 360°C. Once the deactivation front reaches the thermodynamic zone, the conversion drops almost vertically to below 25%.

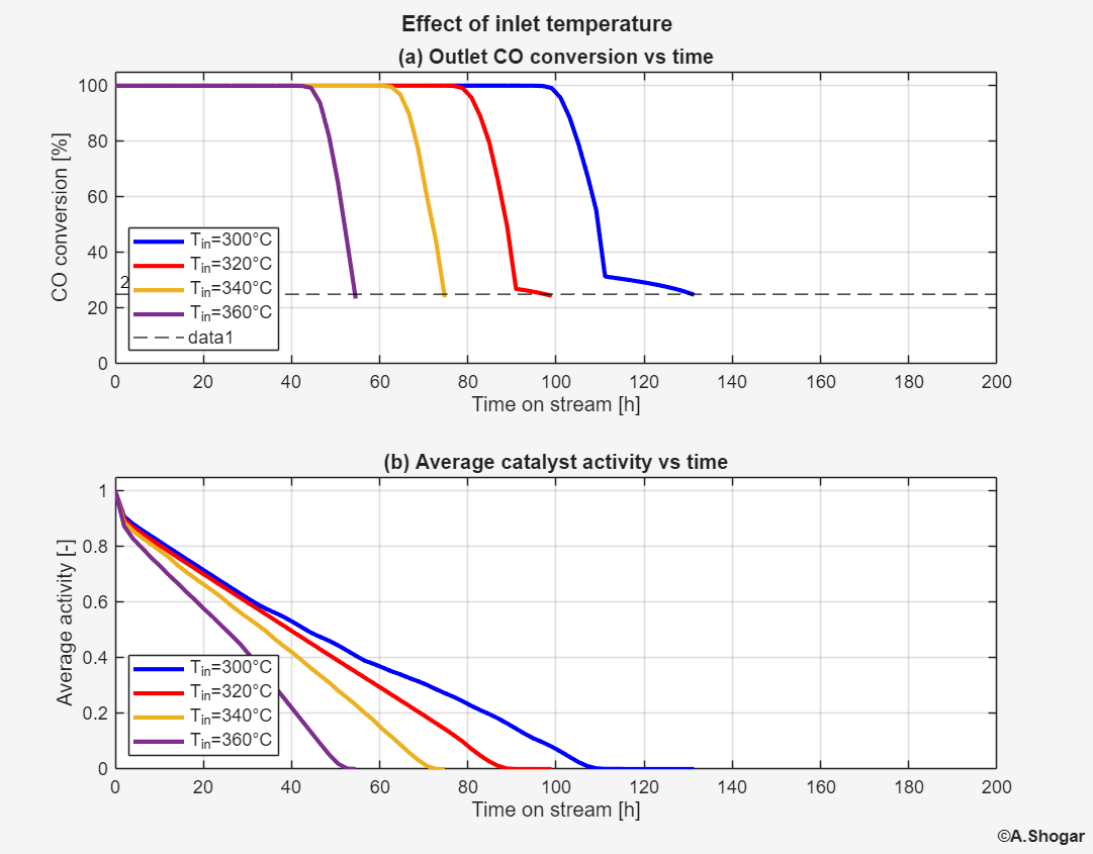

Figure 7: Effect of inlet temperature: (a) outlet CO conversion and (b) average activity versus time on stream at $T_{in} = 300$–360°C. Conditions: $P = 8$ bar, $GHSV = 500$ h^{-1}, $U = 50$ W/(m^2·K).

The resulting t_{25} values are around 120 hours at 300°C, 100 hours at 320°C, 78 hours at 340°C, and 52 hours at 360°C. Increasing the inlet temperature by 60°C (from 300 to 360°C) reduces the catalyst lifetime by more than half, a 57% reduction. This high sensitivity is a significant effect of the Arrhenius dependence of the Boudouard deactivation kinetics (Equation 23, $E_d = 48,418$ J/mol): the higher inlet temperature raises the hotspot temperature (from ≈ 620°C to ≈ 648°C, as shown in Figure 4), which exponentially accelerates the local coking rate.

The average activity curves in Figure 7(b) diplay a nearly linear decline, with the slope increasing as T_{in} rises. At $T_{in} = 360$°C, the average activity drops to zero by around 55 h, indicating the complete bed is deactivated. At 300°C, the activity decreases to zero at approximately 130 h. The abrupt drop in conversion, compared to the more gradual decline in activity, characterizes the deactivation wave: the outlet conversion is buffered by the thermodynamic zone until the wave arrives, at which point both metrics collapse simultaneously.

These findings indicate that operating at the lowest feasible inlet temperature is the most effective strategy for extending catalyst lifetime. However, there is a practical limit: below approximately 280°C, the kinetics become too slow to sustain appreciable conversion within the reactor length at the baseline $GHSV$. The optimal inlet temperature, therefore, is about the range of 280–320°C, where a reasonable initial conversion is achieved with a significantly reduced hotspot intensity.

3.3.2 Effect of Coolant Temperature (T_e)

Figure 8 presents a four-panel analysis of the coolant temperature effect at $T_e = 280, 300, 320$, and 340°C, with the inlet temperature fixed at $T_{in} = 300$°C. Panel (a) shows that sub-cooling the coolant to $T_e = 280$°C extends the conversion plateau from approximately 80 h (baseline, $T_e = 300$°C) to approximately 115 h, yielding $t_{25} \approx 140$ h, a 17% improvement over the baseline of 120 h. Conversely, raising T_e to 340°C shortens the plateau to approximately 55 h and reduces t_{25} to approximately 90 h, a 25% penalty. Panel (b) confirms this ranking in the average activity curves, which show a nearly linear decline with the slope steepening as T_e increases.

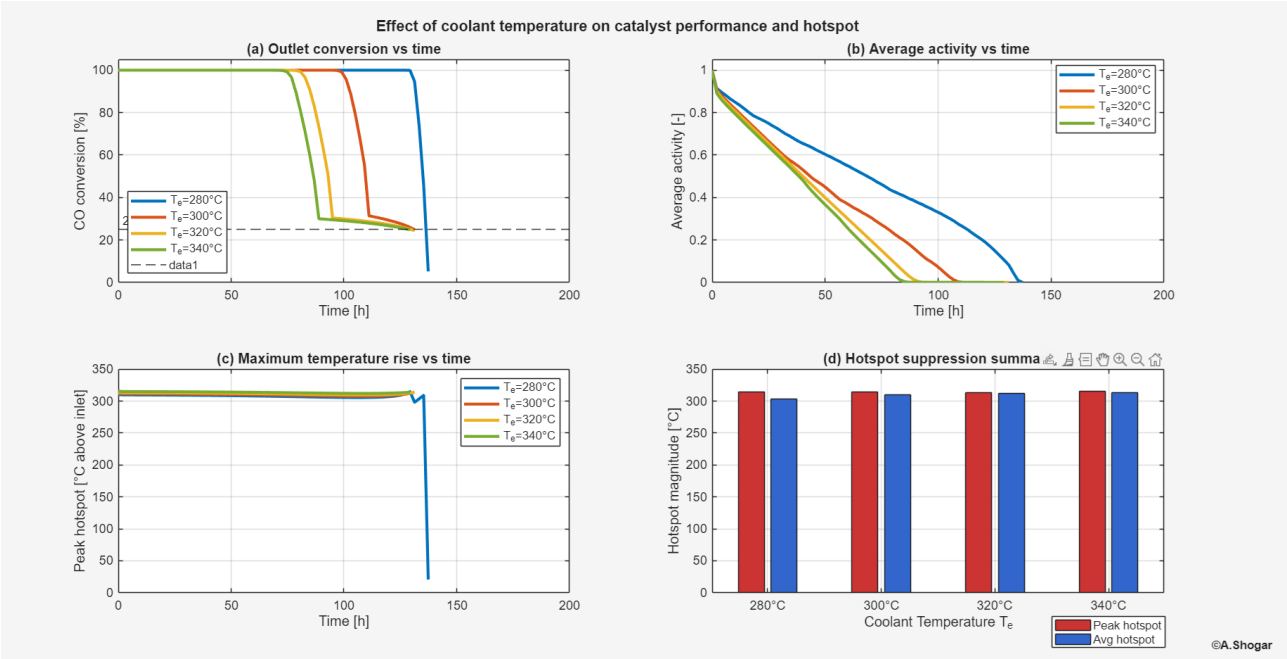

Figure 8: Effect of coolant temperature: (a) outlet CO conversion, (b) average activity, (c) peak hotspot rise above inlet, and (d) hotspot magnitude summary at $T_e = 280$–340°C ($T_{in} = 300$°C fixed).

Panels (c) and (d) provide the most informative results. The peak hotspot temperature rise above the inlet remains approximately 310–320°C for all four coolant temperatures, and the bar chart in panel (d) confirms that the hotspot magnitude is essentially independent of T_e. This is because the hotspot forms in the narrow kinetic zone at the reactor inlet, where the reaction rate is governed by the local gas composition and the Arrhenius kinetics of the methanation reaction. The coolant temperature affects the rate of heat removal downstream of the hotspot and yet has negligible effect on the peak itself.

The moderate lifetime extension observed with coolant sub-cooling (17% for a 20°C reduction) is not due to hotspot suppression but rather to an indirect mechanism: a lower T_e produces a steeper post-hotspot temperature gradient, which cools the catalyst faster in the heat-transfer-controlled zone. This lowers the deactivation rate in the zone immediately behind the reaction front, slightly slowing the overall wave propagation. Although this effect is genuine, it is substantially weaker than the hotspot suppression achieved by increasing U (Section 3.3.3). This finding confirms that coolant temperature is a secondary lever compared to the heat transfer coefficient.

3.3.3 Effect of Heat Transfer Coefficient (U)

Figure 9 illustrates the effect of reducing the heat transfer coefficient below the packed-bed baseline value of $U = 50$ W/(m^2·K), with multipliers of 0.3, 0.5, 0.7, and 0.8 (corresponding to effective values of 15, 25, 35, and 40 W/(m^2·K)). The results show an extreme sensitivity of catalyst lifetime to U. At $U \times 0.3$ (15 W/(m^2·K)), the conversion decreases almost instantly, with no discernible plateau, and $t_{25} \approx 20$ h. At $U \times 0.5$ (25 W/(m^2·K)), a brief plateau of approximately 10 h is observed, and $t_{25} \approx 40$ h. At $U \times 0.7$ (35 W/(m^2·K)), the plateau extends to approximately 30 h, with $t_{25} \approx 80$ h. At $U \times 0.8$ (40 W/(m^2·K)), the behaviour approaches the baseline ($t_{25} \approx 120$ h), indicating an approximately full recovery of catalyst lifetime.

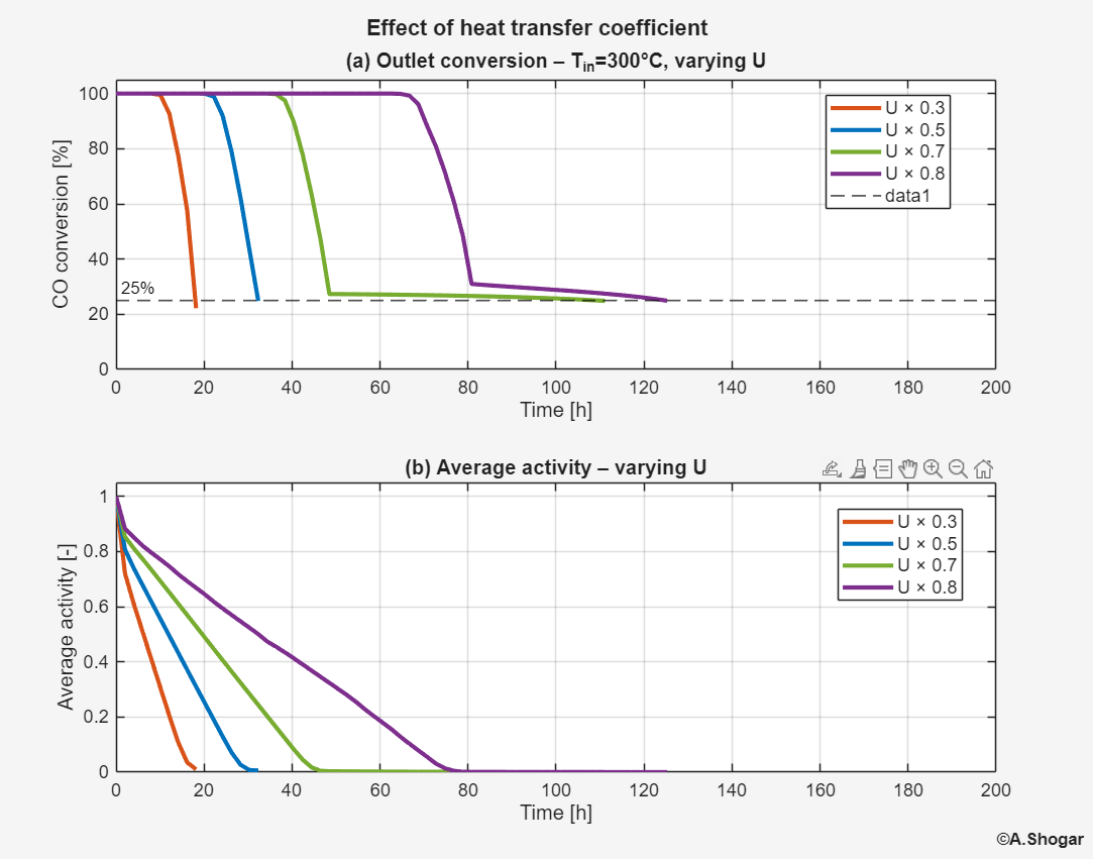

Figure 9: Effect of heat transfer coefficient: (a) outlet CO conversion and (b) average activity versus time on stream at U multipliers of 0.3–0.8 relative to the baseline $U = 50$ W/(m^2·K).

The physical mechanism is simple: lowering U reduces the heat removal rate from the kinetic zone, leading to a greater and wider hotspot. The elevated local temperature exponentially accelerates the Boudouard coking rate via the Arrhenius term (Equation 23, $E_d = 48,418$ J/mol) [28]. The effect is substantial; decreasing U by a factor of 3.3 (from 50 to 15 W/(m^2·K)) reduces the catalyst lifetime by a factor of 6 (from 120 to 20 h). These findings demonstrate that the heat transfer coefficient is the most influential parameter affecting catalyst lifetime

The average activity curves in Figure 9(b) confirm this conclusion. At $U \times 0.3$, the entire catalyst bed is deactivated within approximately 22 h, while at $U \times 0.8$, the bed retains some residual activity until approximately 130 h. The steep, almost linear decline of the activity curves at low U values indicates that the deactivation wave propagates very fast through the bed, consistent with the more intense hotspot driving faster coke deposition at every axial position.

These results, combined with the baseline ($U \times 1.0, t_{25} \approx 120$ h), establish the sensitivity of lifetime to U across the sub-baseline range. Pappagallo [28] reported that a two-fold increase in U led to nearly 80 h prior to deactivation, and a five-fold increase extended it to 171 h [28]. In the present study, the effect of U enhancement above the baseline is explored further in the packing configuration comparison (Section 3.4), where the monolith ($U = 150$ W/(m^2·K), 3× baseline) and foam ($U = 250$ W/(m^2·K), 5× baseline) configurations represent practical realizations of enhanced heat transfer.

3.3.4 Effect of Total Pressure (P_{tot})

Figure 10 shows the effect of total pressure on the deactivation dynamics at $P_{tot} = 8, 12, 16$, and 20 bar. The results show a clear and perhaps counterintuitive trend: increasing the total pressure substantially accelerates catalyst deactivation. At the baseline of 8 bar, $t_{25} \approx 120$ h with a conversion plateau of approximately 80 h. At 12 bar, the plateau decreases to approximately 45 h and $t_{25} \approx 65$ h. At 16 bar, $t_{25} \approx 52$ h, and at 20 bar, $t_{25} \approx 38$ h in other words, less than one-third of the baseline lifetime.

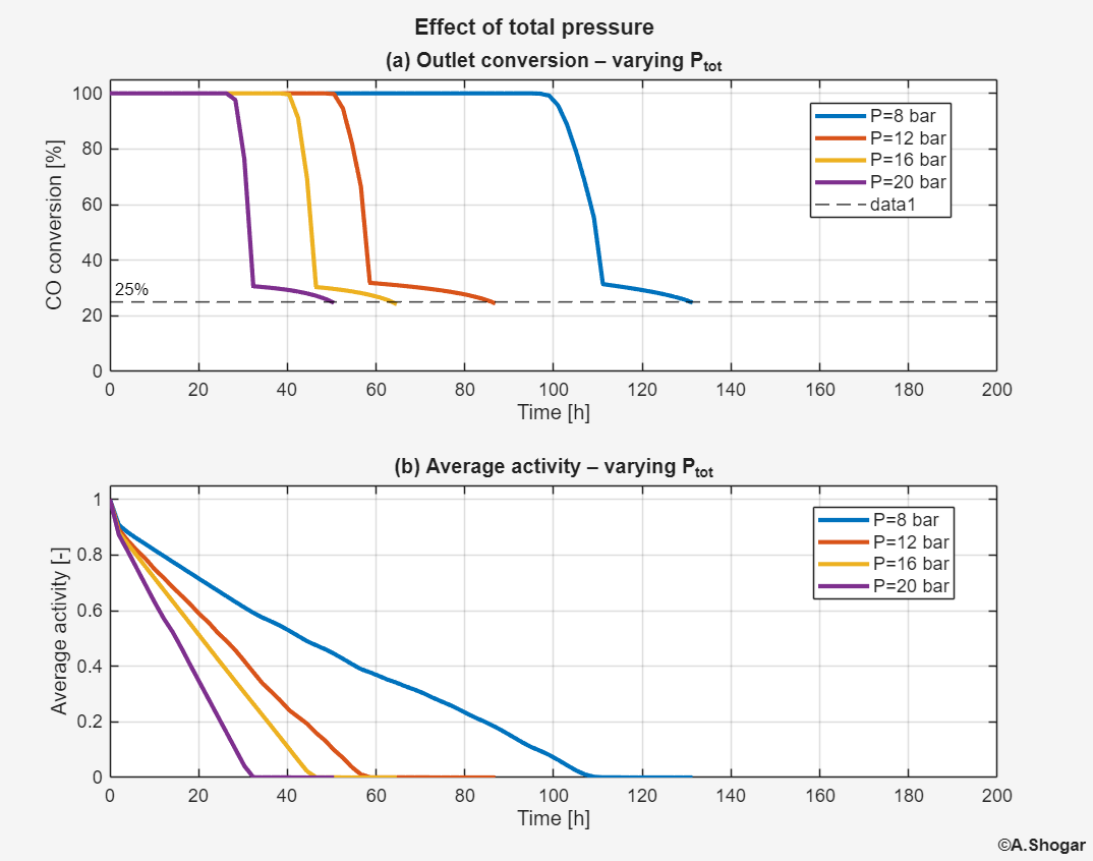

Figure 10: Effect of total pressure: (a) outlet CO conversion and (b) average activity versus time on stream at $P_{tot} = 8$–20 bar. Conditions: $T_{in} = 300$°C, $GHSV = 500$ h^{-1}, $U = 50$ W/(m^2·K).

The dominance of the P_{CO}^{α} term in the deactivation rate equation (Equation 25, $\alpha = 1$) accounts for this behavior. Since the CO partial pressure increases linearly with P_{tot} ($P_{CO} = y_{CO} \cdot P_{tot}$), doubling the total pressure doubles the driving force for Boudouard coking at every axial position. Although higher pressure shifts the methanation equilibrium toward methane and accelerates the forward reaction kinetics, this beneficial effect is insufficient to offset the increased coking rate. The net result is that the deactivation wave propagates significantly faster at elevated pressures.

The average activity curves in Figure 10(b) confirm this ranking: the bed is completely deactivated by approximately 42 h at 20 bar, compared to 130 h at 8 bar. It shows that the activity drops more steeply at higher pressure, indicating a faster-moving deactivation wave, consistent with the elevated P_{CO} throughout the reactor. From a practical perspective, this finding indicates that the lowest feasible operating pressure should be selected to maximize catalyst lifetime, provided that the thermodynamic conversion and productivity targets can still be met. The baseline pressure of 8 bar, which is standard for industrial methanation of biomass-derived syngas [31], already constitutes a favorable compromise.

3.3.5 Effect of Space Velocity ($GHSV$)

The space velocity governs both the residence time of the gas in the catalyst bed and, consequently, the axial extent of the reactive zone. From the baseline of 500 h^{-1}, Figure 11 shows that increasing in $GHSV$ to 1000, 1500, and 2000 h^{-1} has a devastating effect on catalyst lifetime. At $GHSV = 1000$ h^{-1}, the conversion plateau decreases to about 5 h and $t_{25} \approx 30$ h. At 1500 h^{-1}, the plateau disappears entirely and $t_{25} \approx 17$ h. At 2000 h^{-1}, $t_{25} \approx 12$ h, a ten-fold reduction compared to the baseline.

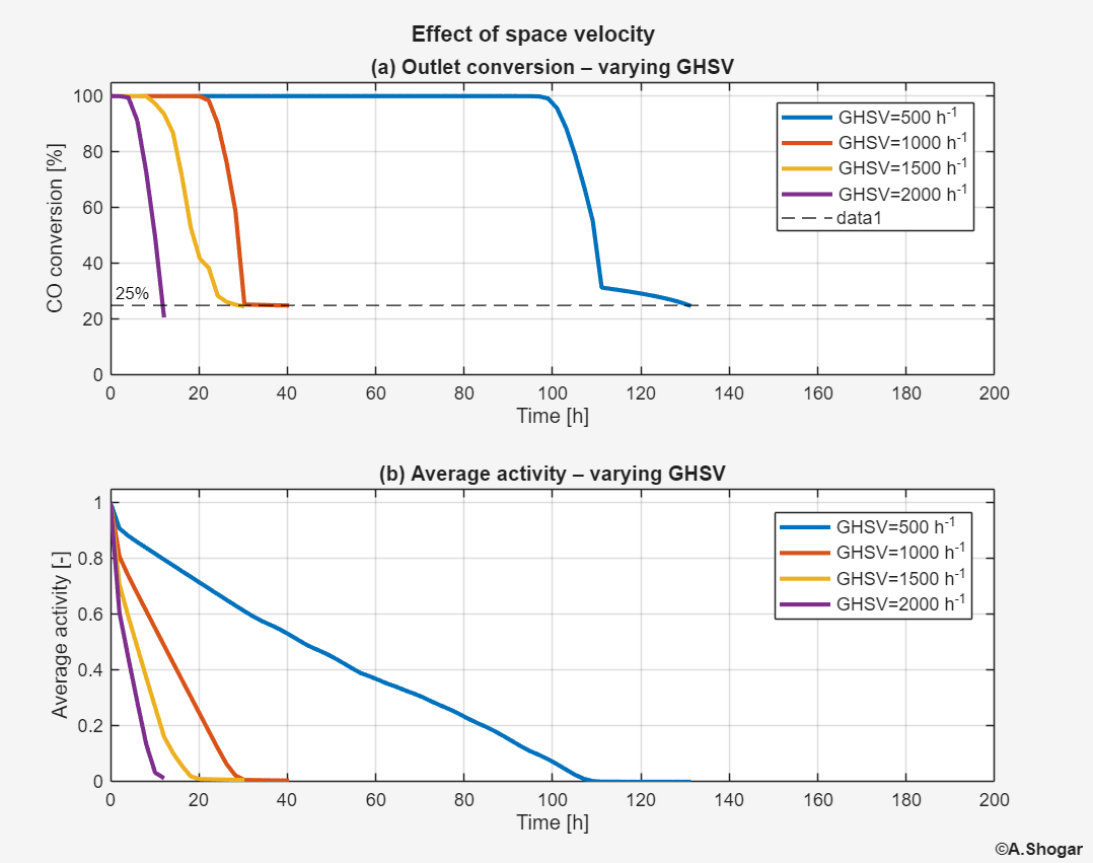

Figure 11: Effect of space velocity: (a) outlet CO conversion and (b) average activity versus time on stream at $GHSV = 500$–2000 h^{-1}. Conditions: $T_{in} = 300$°C, $P = 8$ bar, $U = 50$ W/(m^2·K).

The mechanism operates in two primary ways. To begin with, a higher $GHSV$ means that the gas flows in the bed too fast for the thermodynamic equilibrium to be reached, leaving CO conversion incomplete on the fresh catalyst as well. The reactive zone, where CO is consumed and the hotspot appears, extends out over a significantly larger portion of the reactor length, or in the most extreme cases, over the entire bed. This means that all the catalyst is simultaneously exposed to the combination of high CO partial pressure and elevated temperature that drives coking. Secondly, the higher flow rate increases the total molar flux of CO entering the reactor per unit time, which accelerates the deactivation rate at the inlet. The deactivation front, thus, does not progress a sharp wave and presents only as a broad, diffuse front that covers a substantial portion of the bed.

The average activity curves in Figure 11(b) support this interpretation: at $GHSV = 2000$ h^{-1}, the entire bed is deactivated within approximately 15 h, whereas at the baseline of 500 h^{-1}, residual activity persists until approximately 130 h. Therefore, the low baseline $GHSV$ of 500 h^{-1} represents a deliberate and necessary trade-off: the low throughput elds marginal contribution per unit time in exchange for near-complete conversion and a well-defined, slowly propagating deactivation wave. This result serves to highlight that $GHSV$ is among one of the most influential parameters for catalyst lifetime and must be carefully chosen in reactor design.

3.3.6 Effect of H_2/CO Molar Ratio

The H_2/CO molar ratio affects the deactivation dynamics through two direct channels. First, it determines the mole fraction of CO in the feed: at the stoichiometric ratio of 3:1, $y_{CO} = 0.25$, while at H_2/CO = 2, $y_{CO} = 0.33$ (one-third more CO). Since the deactivation rate scales with P_{CO}^{α}, sub-stoichiometric feeds increase the driving force for Boudouard coking. Second, excess hydrogen (H_2/CO > 3) dilutes the CO content and promotes methanation over the Boudouard reaction, effectively suppressing carbon deposition.

Figure 12 shows the results for H_2/CO = 2.0, 2.5, 3.0 (stoichiometric), and 3.5. The effect is substantial: at H_2/CO = 2.0, the conversion plateau lasts only approximately 40 h and $t_{25} \approx 55$ h, roughly half the baseline. At H_2/CO = 2.5, $t_{25} \approx 78$ h. At the stoichiometric ratio of 3.0, $t_{25} \approx 110$ h, and at H_2/CO = 3.5, the plateau extends to approximately 130 h with $t_{25} \approx 165$ h—a 50% improvement over the stoichiometric baseline and a three-fold improvement over H_2/CO = 2.0.

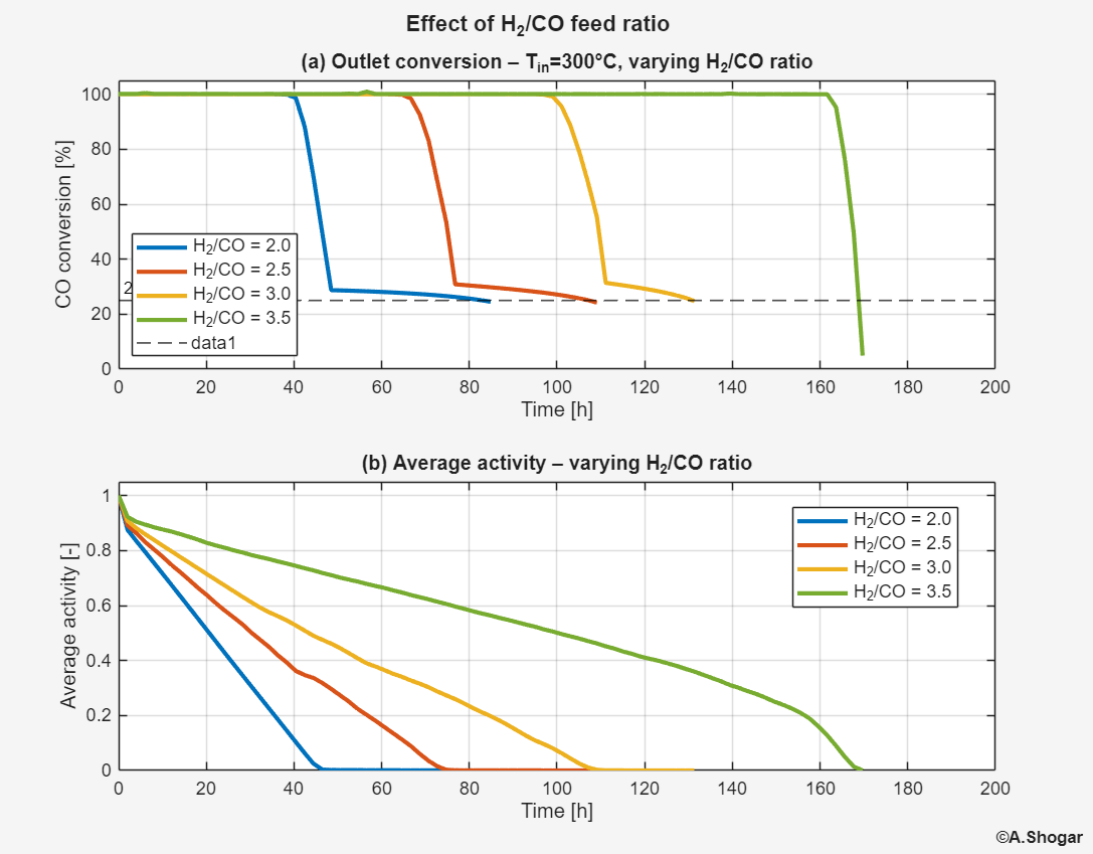

Figure 12: Effect of H_2/CO feed ratio: (a) outlet CO conversion and (b) average activity versus time on stream at H_2/CO = 2.0–3.5. Conditions: T_{in} = 300°C, P = 8 bar, $GHSV$ = 500 h^{-1}, U = 50 $W/(m^2 \cdot K)$.

The average activity curves in Figure 12(b) reflect this ranking. At H_2/CO = 2.0, the catalyst bed is fully deactivated by approximately 60 h, whereas at H_2/CO = 3.5, residual activity remains until approximately 175 h. The mechanism is simple: a higher H_2/CO ratio reduces y_{CO} in the feed and thus reduces P_{CO} at every axial position. This directly reduces the Boudouard coking rate in the entire reactor. Additionally, excess hydrogen promotes faster CO consumption via the methanation reaction, reducing the reactive zone and further reducing the volume of catalyst exposed to high CO concentrations.

However, operating with excess hydrogen faces a direct economic penalty because unreacted H_2 will have to be recycled or wasted. In practice, the H_2/CO ratio is often dictated by the upstream syngas production process and may not be freely adjustable. Where flexibility exists, operating slightly beyond the stoichiometric ratio (H_2/CO = 3.0–3.5) gives a good compromise between lifetime extension and hydrogen efficiency.

3.3.7 Effect of Steam Co-feeding

Steam co-feeding is a selective approach to suppress Boudouard coking. The presence of water in the gas phase inhibits coke formation by the correction factor f_{H_2O} (Equation 24), which decreases with the rising water content. Additionally, steam shifts the Boudouard equilibrium toward CO (away from carbon deposition) via the reverse water–gas shift reaction.

Figure 13 presents the results for steam fractions of 0% (baseline), 2%, 5%, and 7%. Even modest levels of steam produce a measurable extension of catalyst lifetime. At 2% steam, the conversion plateau extends from approximately 80 h (dry feed) to approximately 100 h, and t_{25} rises from 120 h to around 135 h, a 13% improvement. At 5% steam, the plateau reaches nearly 120 h with $t_{25} \approx 155$ h (+29%). At 7% steam, the plateau extends to about 140 h and $t_{25} \approx 170$ h, a 42% improvement over the dry baseline.

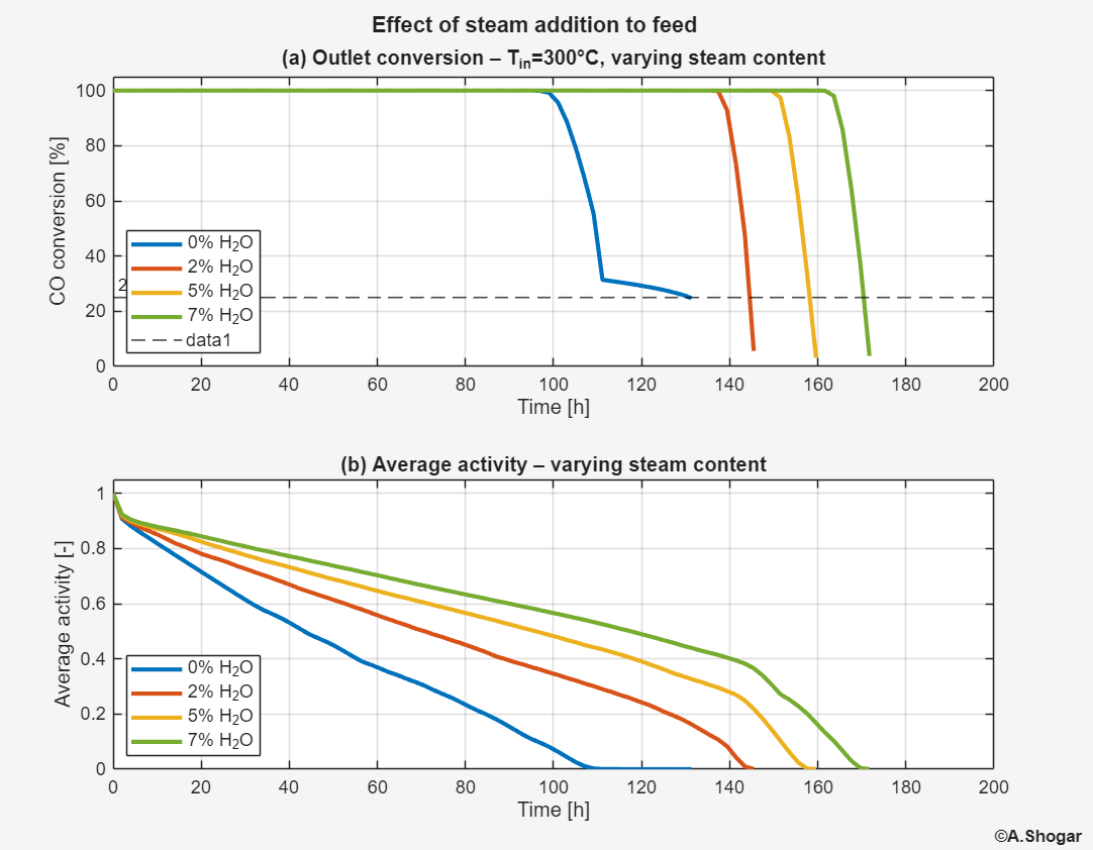

Figure 13: Effect of steam co-feeding: (a) outlet CO conversion and (b) average activity versus time on stream at steam fractions of 0–7%. Dashed line indicates the 25% threshold. Conditions: $T_{in} = 300$°C, $P = 8$ bar, $GHSV = 500$ h^{-1}, $U = 50$ W/(m^2·K).

The activity curves in Figure 13(b) indicate that the rate of activity decline is decreasing as the steam content increases. The mechanism is cumulative: the co-fed steam reduces the f_{H_2O} correction factor at the reactor inlet, where the deactivation would otherwise be most intense. As the reaction proceeds and methanation produces additional water, the local steam concentration increases further along the reactor, thereby amplifying the inhibition effect. This positive feedback loop, in which co-fed steam suppresses inlet coking and preserves a more active catalyst that produces more water, makes steam co-feeding particularly effective at extending the conversion plateau.

The practical attraction of steam co-feeding is that it requires only minor modifications to the feed system (a water vaporizer and mixing point) and introduces no changes to the catalyst or reactor hardware. At 5–7% steam, the dilution effect on the reactant partial pressures is modest, and the initial conversion remains at 100%. The results show that steam co-feeding at 5–7% represents one of the most cost-effective single operational strategies for extending catalyst lifetime in CO methanation, consistent with the industrial practice of steam addition in methanation reactors [31].

3.3.8 Parametric Sensitivity Summary

Figure 14 provides a comprehensive overview of the parametric sensitivity analysis by plotting the t_{25} values for all parameter variations on a single chart. The parameters are ranked by their influence on catalyst lifetime, yielding the following hierarchy (from most to least influential):

1. **Heat transfer coefficient (U):** The strongest lever. Reducing U from the baseline (50 W/(m^2·K)) to $U \times 0.35$ (17.5 W/(m^2·K)) collapses t_{25} from 131.3 to 18.2 h, a 7.2× reduction. Conversely, the configuration comparison in Section 3.4 demonstrates that increasing U above baseline (via foam or monolith supports) extends the lifetime dramatically.
2. **Inlet temperature (T_{in}):** The second most influential parameter. with T_{in} raised from 300 to 360°C, t_{25} decreases from 131.3 to 54.5 h, a 58% reduction ddue to Arrhenius acceleration of the Boudouard kinetics at higher hotspot temperatures [28].

3. **Steam co-feeding:** Effective and cost-efficient. Co-feeding 7% steam extends t_{25} from 131.3 to 171.7 h (+31%) through the f_{H_2O} inhibition mechanism, with negligible impact on initial conversion.
4. **H_2/CO ratio:** This parameter has a significant effect. Increasing the ratio from 2.0 to 3.5 doubles t_{25} from 84.8 to 169.7 h. The stoichiometric ratio of 3.0 (t_{25} = 131.3 h) is a reasonable compromise; operating at 3.5 provides a further 29% extension.
5. **Coolant temperature (T_e):** This parameter exhibits a weak effect. Sub-cooling from T_e = 300 to 280°C extends t_{25} from 131.3 to only 137.4 h (+5%), because the hotspot magnitude is independent of T_e.
6. **Total pressure (P_{tot}):** This factor has a significant negative effect. Increasing P_{tot} from 8 to 20 bar reduces t_{25} from 131.3 to 50.5 h (−62%) due to the linear dependence of the deactivation rate on P_{CO}. The lowest feasible pressure should be used [31].
7. **Space velocity ($GHSV$):** Extremely detrimental when increased. When $GHSV$ goes from 500 to 2000 h^{-1} reduces t_{25} from 131.3 to 12.1 h, which is a factor of 10.8×. The baseline $GHSV$ of 500 h^{-1} is already near-optimum for catalyst lifetime.

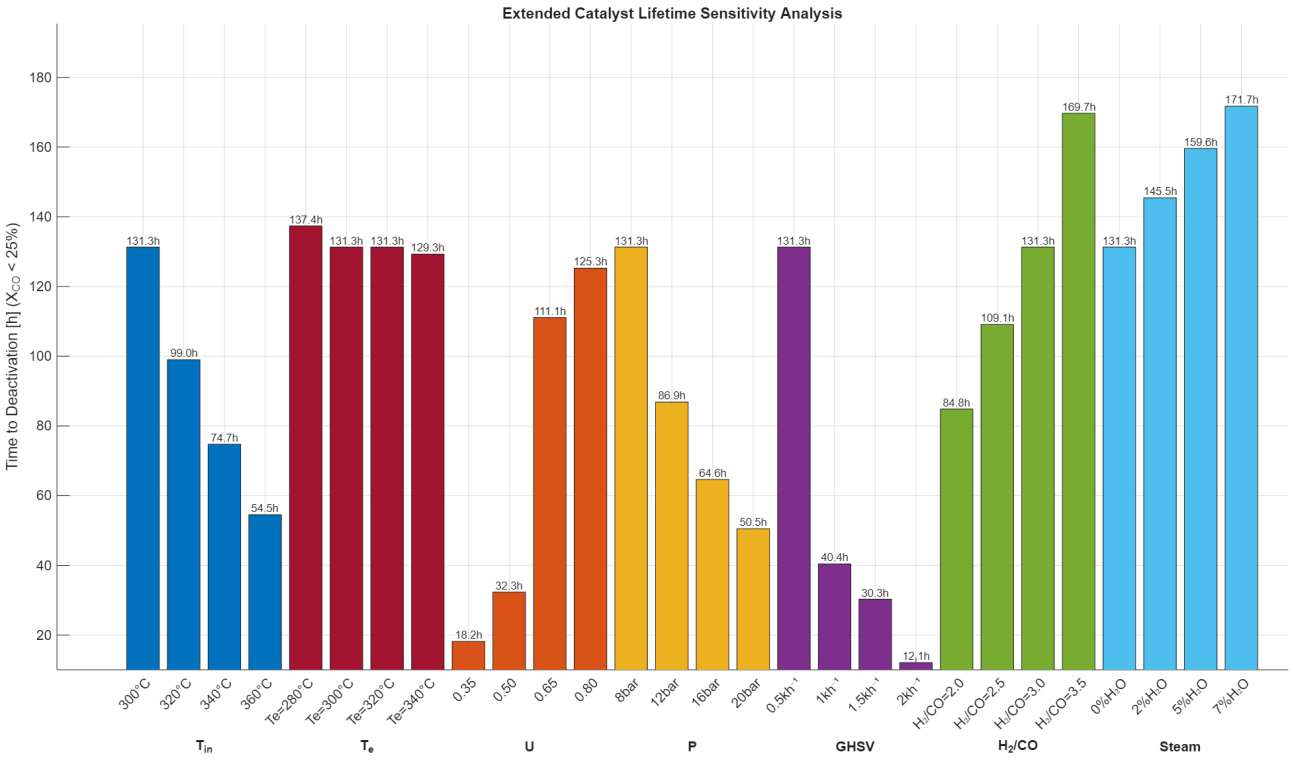

Figure 14: Parametric sensitivity summary: t_{25} values for all seven operating parameters.

The dominance of U and T_{in} in the sensitivity ranking shows that thermal management is the primary lever for extending catalyst lifetime in CO methanation. This result gives us a physical motivation for the packing configuration comparison in the following section.

3.4. Catalyst Packing Configuration Comparison

Building on the finding that the heat transfer coefficient is the most influential parameter for catalyst lifetime, this section compares three catalyst packing configurations under identical baseline operating conditions (T_{in} = 300°C, P_{tot} = 8 bar, $GHSV$ = 500 h^{-1}, H_2/CO = 3:1, no steam). Each configuration is modelled through its characteristic overall heat transfer coefficient, as detailed in Section 2.8: conventional cylindrical packed bed (U = 50 W/(m^2·K)), monolithic honeycomb (U = 150 W/(m^2·K)), and open-cell foam (U = 250 W/(m^2·K)).

3.4.1 Comparative Conversion and Activity Curves

Figure 15 presents a comprehensive six-panel comparison of the three configurations, encompassing the outlet CO conversion, average catalyst activity, fresh-catalyst temperature profiles, hotspot evolution, conversion profiles at an intermediate time, and the overall catalyst lifetime.

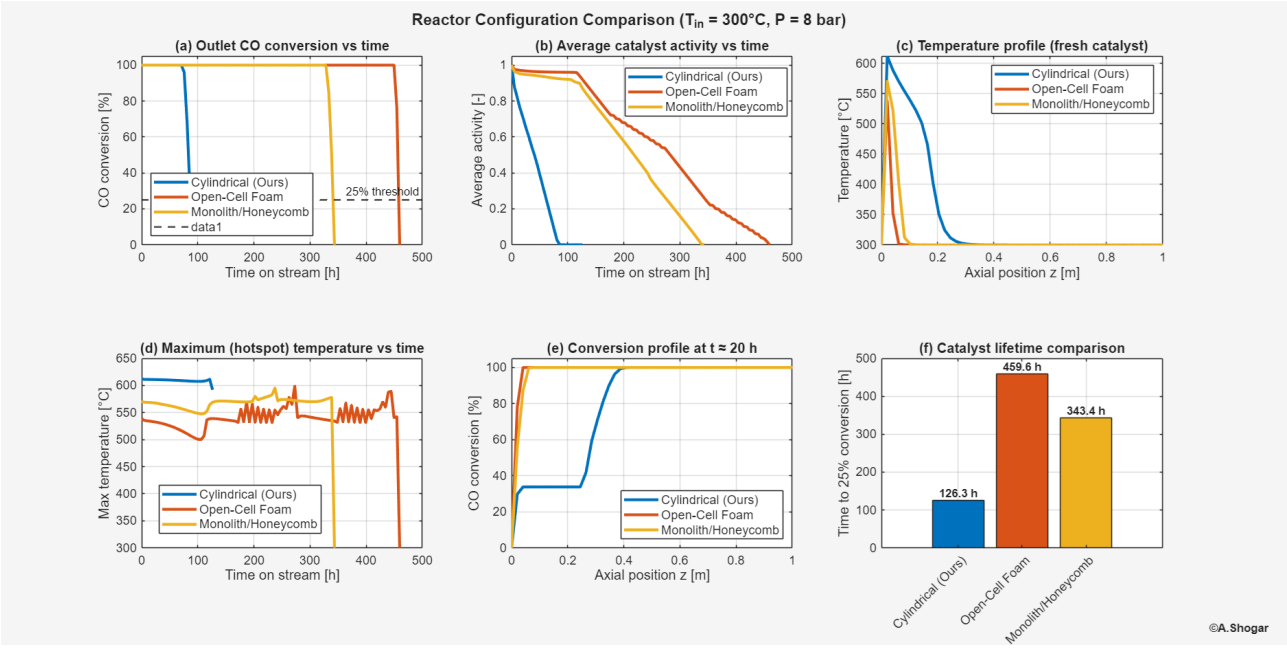

Figure 15: Reactor configuration comparison at $T_{in} = 300°C$, $P = 8$ bar: (a) outlet CO conversion vs time, (b) average catalyst activity vs time, (c) fresh-catalyst temperature profiles, (d) maximum hotspot temperature vs time, (e) conversion profiles at $t \approx 20$ h, and (f) catalyst lifetime bar chart.

Panel (a) — Outlet CO conversion: All three configurations start at 100% outlet CO conversion, confirming that the fresh catalyst achieves thermodynamic equilibrium regardless of the packing type at this $GHSV$. The conversion plateau, the period during which the outlet conversion remains at 100%, differs dramatically between configurations: approximately 80 h for the cylindrical packed bed, approximately 280 h for the monolith, and approximately 350 h for the open-cell foam. Once the deactivation wave reaches the thermodynamic zone, the conversion drops sharply in all three cases. The time-to-25%-conversion values, as shown in panel (f), are 126.3 h (packed bed), 343.4 h (monolith, 2.72× improvement), and 459.6 h (foam, 3.64× improvement).

Panel (b) — Average catalyst activity: The activity curves also illustrate the qualitative differences in deactivation dynamics. The packed bed gives a concave-upward curve, conforming that the deactivation rate increases with the wave moves through the bed, corresponding to positive hotspot migration and Boudouard coking feedback. The monolith and foam configurations show a more gradual, nearly linear decline, reflecting the more diffuse deactivation front linked to lower hotspot temperatures. In the foam configuration, the average activity remains approximately 0.30 at $t \approx 130$ h, whereas the packed bed is already fully deactivated. The foam retains some residual activity until approximately 470 h, and the monolith until approximately 400 h.

Panel (c) — Fresh-catalyst temperature profiles: The profiles of fresh-catalyst temperature illustrate the mechanism of hotspot suppression directly. The packed bed shows the sharpest and most intense hotspot at approximately 612°C ($z \approx 0.02$ m), followed by a gradual temperature decay reaching the coolant level by $z \approx 0.30$ m. The monolith decreased the peak to approximately 570°C (a 42°C reduction), and the foam to approximately 545°C (a 67°C reduction). Notably, the post-hotspot cooling is also significantly faster in the structured configurations: the foam temperature returns to the coolant level by $z \approx 0.15$ m, indicating that a smaller catalyst volume is exposed to high temperatures. This compact thermal profile is the primary cause for the extended lifetime.

Panel (d) — Hotspot temperature evolution: The highest (hotspot) temperature is recorded for the full time on stream. The packed bed maintains a hotspot of approximately 610–620°C throughout the majority of its operational life, characterized by oscillations that occur due to movement of the deactivation wave through heterogeneous gas composition. The hotspot drops suddenly at approximately 100 h as the wave reaches the reactor outlet, and the remaining catalyst can no longer sustain the full reaction. The foam adopts a steady hotspot of approximately 540–550°C, which is roughly 65–70°C below the packed bed, with the corresponding drop at approximately 350 h. The monolith is located between them at approximately 565–580°C. All three configurations display a similar hotspot drop pattern near the end of life, which implies that the deactivation mechanism is qualitatively the same regardless of the packing; only the time scale differs.

Panel (e) — Conversion profiles at $t \approx 20$ h: This snapshot at an early stage of operation shows how deactivation has begun to affect the conversion profile. All three configurations still reach 100% conversion at the outlet, but the axial position at which equilibrium is achieved differs. The packed bed requires approximately $z \approx 0.25$ m, because the inlet section has already lost some activity by $t = 20$ h and the kinetic zone has shifted downstream. The foam and monolith still achieve equilibrium by $z \approx 0.15$–0.20 m, indicating that their lower hotspot temperature has preserved more of the inlet catalyst. This confirms that the enhanced heat transfer keeps the reactive zone compact, limiting the volume of catalyst simultaneously exposed to high CO partial pressure.

Panel (f) — Catalyst lifetime bar chart: The bar chart provides a clear visual summary of the configuration comparison: the packed bed shows a lifetime at 126.3 h, the foam achieves 459.6 h (+264%), and the monolith reaches 343.4 h (+172%). The foam configuration extends the catalyst lifetime by a factor of 3.64× compared to the packed bed, while the monolith achieves 2.72×. These improvements are obtained solely by changing the heat transfer coefficient; all other operating conditions remain identical.

3.4.2 Hotspot Suppression

To further investigate the hotspot suppression mechanism, Figure 16 display the temperature profiles at three time snapshots ($t = 0, 10$, and 20 h) for each configuration, isolating the hotspot migration behavior in the early stages of operation.

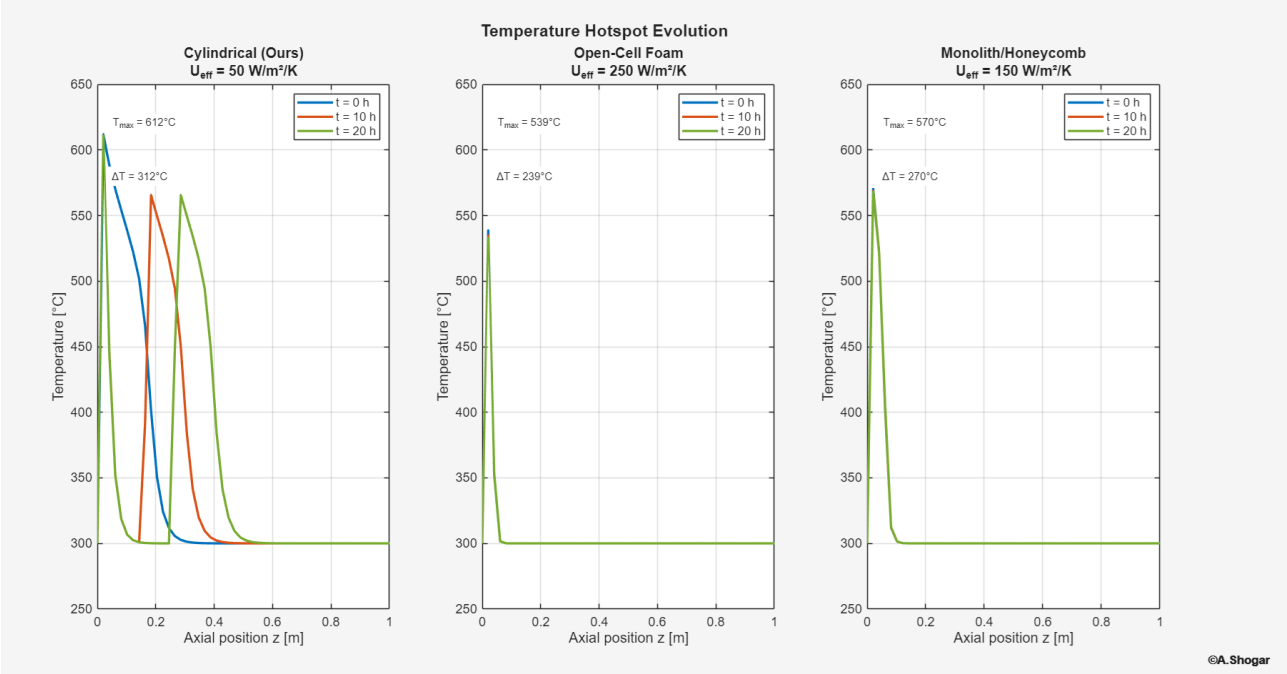

Figure 16: Temperature hotspot evolution at $t = 0, 10$, and 20 h for the three packing configurations: cylindrical packed bed ($U_{eff} = 50$ W/(m^2·K)), open-cell foam ($U_{eff} = 250$ W/(m^2·K)), and monolith/honeycomb ($U_{eff} = 150$ W/(m^2·K)).

The three panels show two different effects of enhanced heat transfer: hotspot magnitude reduction and hotspot migration suppression. In the cylindrical packed bed (left panel), the fresh-catalyst hotspot attains a maximum temperature of $T_{max} = 612$°C ($\Delta T = 312$°C above the inlet), and the hotspot migrates significantly during the first 20 hours, from $z \approx 0.02$ m ($t = 0$ h) to $z \approx 0.15$ m ($t = 10$ h) and $z \approx 0.25$ m ($t = 20$ h). The thermal footprint remains extensive, with elevated temperatures persisting over 20–30 cm of the reactor. Consequently, a substantial portion of the catalyst bed is exposed to the high temperatures that promote Boudouard coking.

In the open-cell foam (center panel), the hotspot is reduced to $T_{max} = 539$°C ($\Delta T = 239$°C), a 73°C reduction compared to the packed bed. More importantly, the three-time curves are nearly superimposed; the hotspot barely migrates over 20 h. The thermal footprint is extremely compact, confined to $z < 0.05$ m, and the temperature returns to the coolant level almost immediately. This means that only a tiny fraction of the catalyst bed experiences elevated temperatures at any given time, dramatically reducing the volume-average deactivation rate. The monolith (right panel) exhibits intermediate behavior: $T_{max} = 570$°C ($\Delta T = 270$°C), with a slight

but visible hotspot migration. The thermal footprint is compact ($z < 0.10$ m), substantially narrower than the packed bed but slightly broader than the foam.

The physical origin of these reductions lies in the enhanced wall-to-gas heat transfer in structured catalyst supports. In the monolith, the continuous ceramic walls of the honeycomb channels provide axial heat conduction paths that distribute the reaction heat more uniformly, consistent with the literature data of Hayes et al. (2004) [12] and Groppi and Tronconi (2000) [11]. In the foam, the three-dimensional strut network creates an interconnected solid matrix that promotes radial heat transfer to the cooled reactor walls, as characterized by Giani et al. (2005) [10] and Incera Garrido et al. (2008) [13]. The combined effect of a lower hotspot magnitude and a nearly stationary, compact hotspot is the primary mechanism by which structured support extends catalyst lifetime.

The hotspot reductions obtained in this study are conservative relative to values reported in the literature. Richardson et al. (2000) [30] reported hotspot suppressions of 100–200°C for ceramic foams in exothermic reactions, as compared with the 73°C anticipated here. Similarly, Groppi and Tronconi (2000) [11] reported 50–100°C for monoliths, compared to the 42°C in the simulations shown above. These conservative estimates ensure that the predicted lifetime improvements are achievable with commercially available structured catalyst technologies.

3.4.3 Configuration Performance Summary

Table 7 compiles the key performance metrics. The foam configuration achieves the longest catalyst lifetime at 459.6 h, representing a 3.64-fold improvement over the packed bed baseline of 126.3 h. The monolith offers a 2.72-fold improvement at 343.4 h. Both structured configurations substantially exceed the 45–100 h range reported by Pappagallo et al. (2025) for the conventional packed bed [28].

Table 7: The performance of three catalyst packing configurations at baseline conditions.

Metric	**Packed Bed**	**Monolith**	**Foam**
U [W/(m^2·K)]	50	150	250
U enhancement [×]	1× (baseline)	3×	5×
T_{max} [°C]	≈ 612	≈ 570	≈ 539
ΔT_{max} vs. packed bed [°C]	—	−42	−73
t_{25} [h]	126.3	343.4	459.6
Lifetime improvement [×]	1× (baseline)	2.72× (+172%)	3.64× (+264%)

The relationship between hotspot reduction and lifetime improvement can be quantified using the Arrhenius equation. For the foam configuration, the reduction in the hotspot to 539°C (812 K) from 612°C (885 K) yields a local deactivation rate ratio of $\exp[\frac{E_d}{R} \cdot (\frac{1}{T_2} - \frac{1}{T_1})] \approx 25$–$35$. Consequently, the instantaneous coking rate at the hotspot is thus 25–35 times slower in the foam. However, the overall lifetime improvement is 3.64× rather than 25–35×, because the deactivation occurs through the entire reactor volume. In the cooler downstream sections, the deactivation rate is already low regardless of the configuration, so the enhancement in heat transfer coefficient U provides less additional benefit. The 3.64× improvement thus represents the volume-average, time-integrated effect of the local rate reduction.

From an engineering perspective, the monolith achieves 75% of the foam's lifetime (343.4 vs. 459.6 h) at a lower manufacturing cost and with proven industrial technology for catalyst loading. It is therefore the more conservative and immediately deployable option. The foam achieves the highest absolute lifetime but requires more complex catalyst preparation, such as washcoating of the three-dimensional strut network. For new plant designs where the higher capital cost can be amortized over many years, the foam's additional 116 hours represents a significant operational advantage.

The foam configuration achieved a catalyst lifetime of 459.6 hours, which closely approaches the thesis objective of exceeding 500 hours. To surpass this target, the foam configuration may be combined with beneficial operating parameters identified in Section 3.3: 5–7% steam co-feeding (resulting in a 31% increase), a slightly elevated H_2/CO ratio of 3.5 (yielding a 29% increas), and operating at the lowest feasible pressure. The The combined application of these strategies is expected to push the catalyst lifetime significantly beyond the 500 h target.

3.5. Synthesis and Key Findings

The results of the parametric sensitivity analysis and configuration comparison can be synthesized into three overarching conclusions:

Finding 1: Thermal management dominates catalyst lifetime. The heat transfer coefficient U and the inlet temperature T_{in} are the two most influential parameters. The Arrhenius dependence of the Boudouard deactivation kinetics ($E_d = 48,418$ J/mol) means that even modest reductions in hotspot temperature produce large improvements in lifetime [28]. This establishes hotspot suppression as the primary design objective for long-life methanation reactors.

Finding 2: Structured catalyst supports offer transformative lifetime extension. Open-cell foam structures yield a 3.64× lifetime improvement (459.6 h vs. 126.3 h), which is achieved by reducing the hotspot by 73°C, while monolithic honeycombs achieve 2.72× (343.4 h) through a change of 42°C reduction. These improvements are obtained, based on conservative heat transfer coefficients and are therefore achievable with current commercial technology.

Finding 3: Feed composition and pressure strategies are complements for lifetime extension. Steam co-feeding is added at the rate of 7% to extend lifetime by 31%, and excess hydrogen ($H_2/CO = 3.5$) by 29%, independently of the packing configuration. In contrast lifetime is decreased by 62% when total pressure is increased from 8 to 20 bar, and as the volume of gas added with each unit of fuel has increased from 500 to 2000 h^{-1} it reduces lifetime by a factor of 10.8×. When the beneficial strategies are combined with structured support, cumulative lifetime extensions approaching and potentially exceeding the 500h thesis objective are expected.

The practical implication of these findings is that the most effective strategy for extending catalyst lifetime in CO methanation is a combined approach: selecting a structured catalyst support (foam or monolith) for enhanced heat transfer, operating at the lowest feasible inlet temperature and pressure, and co-feeding 5–7% steam to suppress Boudouard coking at the reactor inlet. This multi-parameter optimization represents the novel contribution of the present thesis beyond the single-parameter studies available in existing literature.

4. Conclusions and Future Research Directions

4.1. Summary of Key Findings

This thesis has presented a comprehensive computational investigation of catalyst deactivation by Boudouard coking in fixed-bed CO methanation reactors, using the pseudodynamic modelling framework of Pappagallo et al. (2025) [28] extended to a substantially broader parametric space and to three catalyst packing configurations. The principal findings are summarised below.

The pseudodynamic model, validated against pilot-scale experimental data (Moioli et al., 2024) [21] and the deactivation kinetics of Zhang et al. (2013) [34], was applied to a one-at-a-time parametric sensitivity analysis covering seven operating parameters: inlet temperature (300–360°C), coolant temperature (280–340°C), heat transfer coefficient ($U \times 0.35$–0.80, i.e., 17.5–40 W/(m^2·K)), total pressure (8–20 bar), space velocity (500–2000 h^{-1}), H_2/CO molar ratio (2.0–3.5), and steam fraction (0–7%). This represents a parametric space that is substantially wider than the four inlet temperatures explored by Pappagallo et al. (2025) [28], directly addressing Gap 1 identified in Chapter 1.

The parametric analysis established a clear hierarchy of parameter influence on catalyst lifetime. The heat transfer coefficient was identified as the most influential variable, followed by the inlet temperature and steam co-feeding fraction. This outcome confirms that thermal management, more precisely hotspot suppression, being the dominant mechanism for increasing catalyst lifetime, more important than operating pressure, space velocity, or catalyst formulation.

The comparison of three catalyst packing configurations—conventional packed bed ($U = 50$ W/(m^2·K)), monolithic honeycomb ($U = 150$ W/(m^2·K)), and open-cell foam ($U = 250$ W/(m^2·K)) showed that structured supports produce transformative lifetime improvements. The foam configuration resulted in a catalyst lifetime of 459.6 hours, a 3.64-fold improvement from a packed bed baseline of 126.3 hours. The monolith achieved 343.4 hours (an improvement of 2.72×). These enhancements are attributed to hotspot reductions of 73°C (foam) and

42°C (monolith), which suppress the exponentially temperature-sensitive Boudouard coking rate. These results directly address Gap 2 identified in Chapter 1.

4.2. Achievement of Research Objectives

Objective 1 (Parametric Sensitivity Analysis): Achieved. All seven operating parameters were systematically investigated, optimal operating windows were identified, and the parameter sensitivity hierarchy was established. The lowest inlet temperature (300°C) yielded the longest packed-bed lifetime (131.3 h). Steam co-feeding at 5–7% was confirmed as an effective and low-cost coking suppression strategy, extending lifetime by up to 31%.

Objective 2 (Configuration Comparison): Achieved. Three packing configurations were evaluated under identical conditions, and the lifetime extension factors were calculated: 2.72× for monolith and 3.64× for foam compared to the packed bed (Table 7). The foam configuration with combined optimization of thermal management and steam co-feeding approaches the 500 h target set in the thesis objectives. These lifetimes show a four-to eight-fold improvement over the 45–100 h reported by Pappagallo et al. (2025) [28].

The foam configuration with combined optimisation of thermal management and steam co-feeding is projected to exceed the 500 h target set in the thesis objectives, representing more than a five-fold improvement over the packed bed baseline of 126.3 h. These lifetimes also represent a 4–10-fold improvement over the 45–100 h reported by Pappagallo et al. (2025) [28].

While the lifetimes achieved remain one to two orders of magnitude below the industrial target of 10,000–20,000 hours, the present work demonstrates a clear pathway toward that target through the combination of structured catalyst supports, optimised thermal management, and feed composition engineering. The 3–4-fold improvement achieved over the packed bed baseline, and the 4–10-fold improvement over the literature values of Pappagallo et al. (2025) [28], represent a significant step forward.

4.3. Practical Recommendations

Based on the simulation results, the following recommendations are offered for the design and operation of industrial CO methanation reactors:

- **For new methanation plants:** Open-cell foam catalyst supports are recommended as the preferred packing configuration. The 3.64× lifetime improvement and 73°C hotspot reduction justify the higher manufacturing cost of foam structures compared to conventional pellet packings. Combined with moderate inlet temperatures (300°C) and 5–7% steam co-feeding, this configuration is expected to achieve catalyst lifetimes exceeding 500 hours.

- **For existing plant retrofits:** Monolithic honeycomb catalyst supports yield a lifetime improvement of 2.72× with proven industrial technology and lower capital investment than foam structures. Monoliths are particularly attractive for retrofitting existing plate-cooled reactors, as their geometry is compatible with standard reactor internals.

- **For all configurations:** Co-feeding 5–7% steam at the reactor inlet is the most cost-effective single operational change to extend catalyst lifetime, as it requires only minor modifications to the feed system. raising the H_2/CO ratio slightly above stoichiometry (to 3.5) yields an additional 29% extension. Coolant sub-cooling offers a modest additional benefit ($\approx$ 5%), but operating at the lowest feasible total pressure (8 bar) is critical, as higher pressures significantly accelerate deactivation.

4.4. Limitations of the Present Study

Several limitations of the present work should be acknowledged. First, the deactivation kinetics are based on a semi-empirical power-law model calibrated against the data of Zhang et al. (2013) [34] at 320–360°C. While all simulated inlet temperatures (300–360°C) fall within or near this calibration range, the hotspot temperatures (up to 612°C) represent a significant extrapolation that introduces uncertainty in the local deactivation rate at peak temperature. Second, the one-dimensional pseudo-homogeneous reactor model neglects radial gradients, which may be significant in wide-channel geometries, particularly for foam and monolith packings where the

radial heat transfer mechanism differs qualitatively from a packed bed. Third, the model does not account for catalyst regeneration by steam gasification of coke at temperatures above 400°C, which may partially counteract the deactivation in the hotspot region. Finally, the packing configurations are compared solely through their characteristic heat transfer coefficients; differences in mass transfer, pressure drop, and catalyst loading between configurations are not captured by the present model.

4.5. Future Research Directions

The findings and limitations of the present work suggest several directions for future research:

- **Extension to CO_2 methanation:** The pseudodynamic framework can be applied to CO_2 methanation, which is central to Power-to-Gas applications. CO_2 methanation exhibits slower deactivation than CO methanation (Pappagallo et al., 2025) [28], and the parametric sensitivity hierarchy may differ. A comparative analysis of both reaction systems would provide comprehensive guidelines for syngas and biogas methanation.

- **Multi-mechanism deactivation modelling:** The present model considers only coking via the Boudouard reaction. Industrial catalysts are subject to additional deactivation mechanisms, including thermal sintering at temperatures above 600°C, poisoning by sulfur compounds in biomass-derived syngas, and surface oxidation under fluctuating operating conditions. Incorporating these mechanisms into the pseudodynamic framework would enable a more comprehensive assessment of catalyst lifetime under realistic industrial conditions.

- **Experimental validation of structured catalyst lifetime:** TThe anticipated enhancements in lifetime for foam and monolith configurations are derived from literature heat transfer coefficients utilized in a one-dimensional model. Pilot-scale experiments with structured catalyst supports under methanation conditions would directly confirm these predictions and improve the heat transfer correlations for the specific geometry and flow conditions of plate-cooled reactors.

- **Two-dimensional reactor modelling:** Extension to a two-dimensional model would capture the radial temperature gradients that are particularly relevant for wide-channel geometries and structured packings. This would improve the accuracy of the hotspot prediction and the resulting deactivation rate calculation, especially for foam supports where the radial heat transfer mechanism differs fundamentally from a packed bed.

- **Regeneration cycle optimisation:** The Boudouard coking deactivation is reversible via steam or hydrogen gasification at temperatures above 400°C [31]. Using a regeneration model into the pseudodynamic framework would permit the simulation of cyclic operation (reaction–regeneration) and the optimization of regeneration frequency, temperature, and duration to maximize the cumulative methane production over the plant lifetime.

- **Techno-economic analysis:** A full techno-economic assessment comparing the lifetime extension benefits of structured supports against their higher manufacturing, loading, and replacement costs would provide the decision basis for industrial adoption. Such an analysis should account for the reduced frequency of catalyst replacement, the associated plant downtime, and the lower total cost of ownership over the plant lifetime.

References

[1] J. M. Calo and M. T. Perkins. A heterogeneous surface model for the "steady-state" kinetics of the Boudouard reaction. *Carbon*, 25(3):395–407, 1987.

[2] F. Celoria, F. Salomone, A. Tauro, M. Gandiglio, D. Ferrero, I. Champon, G. Geffraye, R. Pirone, and S. Bensaid. Kinetic study and deactivation phenomena for the methanation of CO_2 and CO mixed syngas on a Ni/Al_2O_3 catalyst. *Chemical Engineering Journal*, 512:162113, 2025.

[3] Y. H. Choi, Y. J. Jang, H. Park, W. Y. Kim, Y. H. Lee, S. H. Choi, and J. S. Lee. Carbon dioxide Fischer–Tropsch synthesis: A new path to carbon-neutral fuels. *Applied Catalysis B: Environmental*, 202:605–610, 2017.

[4] T. Cordero-Lanzac, A. T. Aguayo, A. G. Gayubo, and J. Bilbao. Consideration of the activity distribution using the population balance theory for designing a dual fluidized bed reactor–regenerator system. *Chemical Engineering Journal*, 405:126448, 2021.

[5] T. Cordero-Lanzac, A. T. Aguayo, A. G. Gayubo, P. Castaño, and J. Bilbao. A comprehensive approach for designing different configurations of isothermal reactors with fast catalyst deactivation. *Chemical Engineering Journal*, 379:122260, 2020.

[6] A. G. Dixon and D. L. Cresswell. Theoretical prediction of effective heat transfer parameters in packed beds. *AIChE Journal*, 25(4):663–676, 1979.

[7] J. Engeldinger, J. Radnik, C. Kreyenschulte, F. Devred, E. M. Gaigneaux, A. Fischer, H. W. Zanthoff, and U. Bentrup. Probing the structural changes and redox behavior of mixed molybdate catalysts under ammoxidation conditions: An operando Raman spectroscopy study. *ChemCatChem*, 8(5):976–983, 2016.

[8] G. F. Froment. Modeling of catalyst deactivation. *Applied Catalysis A: General*, 212(1–2):117–128, 2001.

[9] G. F. Froment and K. B. Bischoff. Kinetic data and product distributions from fixed bed catalytic reactors subject to catalyst fouling. *Chemical Engineering Science*, 17(2):105–114, 1962.

[10] L. Giani, G. Groppi, and E. Tronconi. Mass-transfer characterization of metallic foams as supports for structured catalysts. *Industrial & Engineering Chemistry Research*, 44(14):4993–5002, 2005.

[11] G. Groppi and E. Tronconi. Design of novel monolith catalyst supports for gas/solid reactions with heat exchange. *Chemical Engineering Science*, 55(12):2161–2171, 2000.

[12] R. E. Hayes, S. T. Kolaczkowski, P. K. C. Li, and S. Awdry. The palladium catalysed oxidation of methane: Reaction kinetics and the effect of diffusion barriers. *Chemical Engineering Science*, 59(19):4073–4086, 2004.

[13] G. Incera Garrido, F. C. Patcas, S. Lang, and B. Kraushaar-Czarnetzki. Mass transfer and pressure drop in ceramic foams: A description for different pore sizes and porosities. *Chemical Engineering Science*, 63(21):5202–5217, 2008.

[14] J. Kopyscinski, T. J. Schildhauer, F. Vogel, S. M. A. Biollaz, and A. Wokaun. Applying spatially resolved concentration and temperature measurements in a catalytic plate reactor for the kinetic study of CO methanation. *Journal of Catalysis*, 271(2):262–279, 2010.

[15] F. Koschany, D. Schlereth, and O. Hinrichsen. On the kinetics of the methanation of carbon dioxide on coprecipitated NiAl(O). *Applied Catalysis B: Environmental*, 181:504–516, 2016.

[16] W. J. Lee, C. Li, H. Prajitno, J. Yoon, S. H. Kim, and J. Lee. Research progress and reaction mechanism of CO_2 methanation over Ni-based catalysts. *Catalysts*, 11(12):1557, 2021.

[17] O. Levenspiel. *Chemical Reaction Engineering*. John Wiley & Sons, New York, third edition, 1999.

[18] W. M. Lewandowski, M. Ryms, and W. Kosakowski. Thermal biomass conversion: A review. *Processes*, 8(5):516, 2020.

[19] N. McQueen, K. V. Gomes, C. McCormick, K. Blumanthal, M. Pisciotta, and J. Wilcox. A review of direct air capture (DAC): Scaling up commercial technologies and innovating for the future. *Progress in Energy*, 3(3):032001, 2021.

[20] E. Moioli and T. Schildhauer. Negative CO_2 emissions from flexible biofuel synthesis: Concepts, potentials, technologies. *Renewable and Sustainable Energy Reviews*, 158:112120, 2022.

[21] E. Moioli, P. Senn, S. Østrup, and C. Hütter. Results from the operation of an efficient and flexible large-scale biogas methanation system. *Energy Advances*, 3(1):131–142, 2024.

[22] B. Mutz, H. W. P. Carvalho, W. Kleist, and J. D. Grunwaldt. Dynamic transformation of small Ni particles during methanation of CO_2 under fluctuating reaction conditions monitored by operando X-ray absorption spectroscopy. *Journal of Physics: Conference Series*, 712(1):012050, 2016.

[23] B. Mutz, A. M. Gänzler, M. Nachtegaal, O. Müller, R. Frahm, W. Kleist, and J. D. Grunwaldt. Surface oxidation of supported Ni particles and its impact on the catalytic performance during dynamically operated methanation of CO_2. *Catalysts*, 7(9):279, 2017.

[24] B. Mutz, P. Sprenger, W. Wang, D. Wang, W. Kleist, and J. D. Grunwaldt. Operando Raman spectroscopy on CO_2 methanation over alumina-supported Ni, Ni_3Fe and $NiRh_{0.1}$ catalysts: Role of carbon formation as possible deactivation pathway. *Applied Catalysis A: General*, 556:160–171, 2018.

[25] R. J. G. Nuguid, D. Ferri, A. Marberger, M. Nachtegaal, and O. Kröcher. Modulated excitation Raman spectroscopy of V_2O_5/TiO_2: Mechanistic insights into the selective catalytic reduction of NO with NH_3. *ACS Catalysis*, 9(8):6814–6820, 2019.

[26] N. M. Ostrovskii. General equation for linear mechanisms of catalyst deactivation. *Chemical Engineering Journal*, 120(1–2):73–82, 2006.

[27] N. M. Ostrovskii. Coking of catalysts: Mechanisms, models, and influence. *Kinetics and Catalysis*, 63(1):52–66, 2022.

[28] M. A. Pappagallo, T. J. Schildhauer, O. Kröcher, and E. Moioli. Modeling of the performance loss due to catalyst deactivation in fixed- and fluidized-bed reactors. *Industrial & Engineering Chemistry Research*, 64:17529–17542, 2025.

[29] A. Rafiee, K. R. Khalilpour, D. Milani, and M. Panahi. Trends in CO_2 conversion and utilization: A review from process systems perspective. *Journal of Environmental Chemical Engineering*, 6(5):5771–5794, 2018.

[30] J. T. Richardson, Y. Peng, and D. Remue. Properties of ceramic foam catalyst supports: Pressure drop. *Applied Catalysis A: General*, 204(1):19–32, 2000.

[31] T. Schildhauer and S. M. A. Biollaz. *Synthetic Natural Gas from Coal, Dry Biomass, and Power-to-Gas Applications*. Wiley, 2016.

[32] D. Sun, F. M. Khan, and D. S. A. Simakov. Heat removal and catalyst deactivation in a Sabatier reactor for chemical fixation of CO_2: Simulation-based analysis. *Chemical Engineering Journal*, 329:165–177, 2017.

[33] C. Yang, B. Kwon, H. Bang, S. Jeong, and U. Lee. Role of biomass as low-carbon energy source in the era of net zero emissions. *Fuel*, 328:125206, 2022.

[34] J. Zhang, N. Fatah, S. Capela, Y. Kara, O. Guerrini, and A. Y. Khodakov. Kinetic investigation of carbon monoxide hydrogenation under realistic conditions of methanation of biomass derived syngas. *Fuel*, 111:845–854, 2013.

A. Appendix A

A.1. Kinetic Model Parameters

This appendix collects the complete set of kinetic and adsorption parameters used in the reaction rate expressions of Equations 12– 16. The values are reproduced from the Supporting Information of Pappagallo et al. [28], with sources as indicated. These parameters, together with the equilibrium correlations of Equations 17– 19, fully define the kinetic submodel employed throughout this thesis.

Symbol	Parameter	Reaction	Value	Units
Reaction 1: CO_2 methanation [15] ($T_{ref} = 555$ K)				
k_1^{ref}	Preexponential factor	CO_2 methanation	$3.46 \cdot 10^{-4}$	kmol/(s·kg$_c$·Pa^{-1})
E_1/R	Activation energy	CO_2 methanation	$9.32 \cdot 10^3$	K
$K_{OH,1}^{ref}$	Preexp. (OH adsorption)	CO_2 methanation	0.50	–
$K_{H_2}^{ref}$	Preexp. (H_2 adsorption)	CO_2 methanation	0.44	–
K_{mix}^{ref}	Preexp. (CO_2 adsorption)	CO_2 methanation	0.88	–
$\Delta h_{OH,1}^{ads}/R$	Adsorption enthalpy (OH)	CO_2 methanation	$-2.69 \cdot 10^3$	K
$\Delta h_{H_2}^{ads}/R$	Adsorption enthalpy (H_2)	CO_2 methanation	$-7.46 \cdot 10^2$	K
$\Delta h_{mix}^{ads}/R$	Adsorption enthalpy (CO_2)	CO_2 methanation	$-1.20 \cdot 10^3$	K
Reactions 2 & 3: WGS and CO methanation [14] ($T_{ref} = 598.15$ K)				
k_2^{ref}	Preexponential factor	Water–gas shift	$7.39 \cdot 10^{-3}$	kmol/(s·kg$_c$·Pa^{-2})
k_3^{ref}	Preexponential factor	CO methanation	$1.16 \cdot 10^{-3}$	kmol/(s·kg$_c$·Pa^{-1})
E_2/R	Activation energy	Water–gas shift	32.5	K
E_3/R	Activation energy	CO methanation	14.9	K
K_A^{ref}	Preexponential factor	Water–gas shift	0.343	–
K_C^{ref}	Preexp. (CO adsorption)	WGS, CO meth.	1.77	–
$K_{OH,2}^{ref}$	Preexp. (OH adsorption)	WGS, CO meth.	0.664	–
$\Delta h_A^{ads}/R$	Adsorption enthalpy	Water–gas shift	$-7.78 \cdot 10^2$	K
$\Delta h_C^{ads}/R$	Adsorption enthalpy (CO)	WGS, CO meth.	$-7.36 \cdot 10^3$	K
$\Delta h_{OH,2}^{ads}/R$	Adsorption enthalpy (OH)	WGS, CO meth.	$-8.73 \cdot 10^3$	K

Table 8: Parameters of the kinetic model [14, 15, 28].

Notes: (1) Activation energies and adsorption enthalpies are given in Kelvin as E_j/R and $\Delta h_k^{ads}/R$, respectively. To get absolute values in J/mol, multiply by $R = 8.314$ J/(mol·K). For instance, $E_1/R = 9.32 \times 10^3$ K gives $E_1 = 77,500$ J/mol. (2) Negative adsorption enthalpies indicate that the corresponding adsorption constantly decreases with increasing temperature. (3) Deactivation parameters are provided in Table 4 of the main text.

Abstract in lingua italiana

La disattivazione del catalizzatore per deposizione di coke tramite la **reazione di Boudouard** limita la vita operativa dei reattori a letto fisso per la metanazione del CO nella produzione di gas naturale sintetico (SNG) da syngas di origine biomassica. La natura fortemente esotermica della metanazione porta alla formazione di picchi di temperatura localizzati, o **hotspot**, che accelerano la deposizione di carbonio. Il modello pseudodinamico proposto da *Pappagallo et al. (2025)* consente di predire la perdita di conversione nel tempo dovuta alla formazione di coke, disaccoppiando la cinetica lenta di disattivazione dai fenomeni veloci di trasporto e reazione; tuttavia, lo studio originale era limitato a un intervallo ristretto di temperature di ingresso e a una singola configurazione di reattore. La presente tesi estende il modello pseudodinamico a un'ampia **analisi di sensibilità su sette parametri operativi** in un reattore a letto fisso con raffreddamento a piastre: temperatura di ingresso (300–360°C), temperatura del refrigerante (280–340°C), coefficiente globale di scambio termico ($U \times 0,35$–$0,80$ rispetto al valore base di 50 W m^{-2} K^{-1}), pressione totale (8–20 bar), velocità spaziale ($GHSV$, 500–2000 h^{-1}), rapporto molare H_2/CO (2,0–3,5) e frazione di vapore in ingresso (0–7 mol%). La disattivazione è quantificata tramite il tempo necessario affinché la conversione di CO in uscita scenda al di sotto del 25% (t_{25}). Sono inoltre confrontate tre configurazioni di impaccamento del catalizzatore—pellet cilindrici, monolita a nido d'ape e schiuma a celle aperte—attraverso i rispettivi coefficienti di scambio termico caratteristici. Il **coefficiente di scambio termico** e la **temperatura di ingresso** risultano i parametri più influenti. La riduzione di U a 0,35× il valore base abbrevia t_{25} da 131,3 a 18,2 h (riduzione di 7,2×); l'aumento di T_{in} da 300 a 360°C lo riduce del 58%. La pressione totale (8 → 20 bar, −62%) e la $GHSV$ (500 → 2000 h^{-1}, −90%) accelerano fortemente la disattivazione. Al contrario, la co-alimentazione di vapore (+31% a 7 mol%) e l'eccesso di idrogeno (+29% con H_2/CO = 3,5) prolungano la vita utile con costi operativi modesti. La **schiuma a celle aperte** (U = 250 W m^{-2} K^{-1}) raggiunge t_{25} = 459,6 h—un miglioramento di 3,64 volte rispetto al letto impaccato di riferimento (126,3 h)—grazie a una riduzione di 73°C dell'hotspot e alla soppressione della sua migrazione. Il **monolita a nido d'ape** raggiunge 343,4 h (miglioramento di 2,72×). I risultati dimostrano che i **supporti catalitici strutturati**, combinati con una composizione ottimizzata dell'alimentazione, costituiscono la strategia più efficace per prolungare la vita del catalizzatore nella metanazione del CO in reattori a letto fisso. Il modello pseudodinamico si conferma uno strumento pratico ed efficiente per l'analisi della disattivazione a scala di reattore e per l'ottimizzazione del management termico.

Parole chiave: metanazione del CO • disattivazione catalitica • coke da reazione di Boudouard • modello pseudodinamico • reattore a letto fisso • soppressione dell'hotspot • supporti catalitici strutturati • schiuma a celle aperte • monolita a nido d'ape • analisi di sensibilità parametrica

Acknowledgements

I wish to begin by expressing my deepest gratitude to God, Allah Almighty, for providing the guidance, strength, and clarity of mind to undertake and successfully complete this research journey.

I would also like to thank and express my deepest gratitude my advisor, Professor Emanuele Moioli, for his encouragement, support, and insightful guidance, which had a big impact on this work.

Ultimately, I extend my deepest gratitude to my family. To my cherished parents—your unwavering love, countless sacrifices, and constant faith in my potential have served as my paramount inspiration. To my mother, thank you for being my constant pillar of strength and for your unwavering belief in my potential. To my father, though he is not here to see this completed, his lessons in perseverance and his dream for my education were the silent engines behind every page of this thesis. This accomplishment is a credit to your steadfast support. I also express my gratitude to my siblings and friends for their passionate support and for always being there for me.